remote sensing

MDPI

Article

Study of the Preparation Phase of Turkey's Powerful Earthquake (6 February 2023) by a Geophysical Multi-Parametric Fuzzy Inference System

Mehdi Akhoondzadeh [1,*] and Dedalo Marchetti [2]

[1] Photogrammetry and Remote Sensing Department, School of Surveying and Geospatial Engineering, College of Engineering, University of Tehran, North Amirabad Ave., Tehran 1417614411, Iran
[2] College of Instrumentation and Electrical Engineering, Jilin University, Changchun 130061, China; dedalomarchetti@jlu.edu.cn
* Correspondence: makhonz@ut.ac.ir

Abstract: On 6 February 2023, a powerful earthquake at the border between Turkey and Syria caused catastrophic consequences and was, unfortunately, one of the deadliest earthquakes of the recent decades. The moment magnitude of the earthquake was estimated to be 7.8, and it was localized in the Kahramanmaraş region of Turkey. This article aims to investigate the behavior of more than 50 different lithosphere–atmosphere–ionosphere (LAI) anomalies obtained from satellite data and different data services in a time period of about six months before the earthquake to discuss the possibility of predicting the mentioned earthquake by an early warning system based on various geophysical parameters. In this study, 52 time series covering six months of data were acquired with: (i) three identical satellites of the Swarm constellation (Alpha (A), Bravo (B) and Charlie (C); and the analyzed parameters: electron density (Ne) and temperature (Te), magnetic field scalar (F) and vector (X, Y and Z) components); (ii) the Google Earth Engine (GEE) platform service data (including ozone, water vapor and surface temperature), (iii) the Giovanni data service (including the aerosol optical depth (AOD), methane, carbon monoxide and ozone); and (iv) the USGS earthquake catalogue (including the daily seismic rate and maximum magnitude for each day), around the location of the seismic event from 1 September 2022 to 17 February 2023, and these were analyzed. The results show that the number of seismic anomalies increased since about 33 days before the earthquake and reached a peak, i.e., the highest number, one day before. The findings of implementing the proposed predictor based on the Mamdani fuzzy inference system (FIS) emphasize that the occurrence of a powerful earthquake could be predicted from about nine days to one day before the earthquake due to the clear increase in the number of seismo-LAI anomalies. However, this study has still conducted a posteriori, knowing the earthquake's epicenter and magnitude. Therefore, based on the results of this article and similar research, we emphasize the urgency of the creation of early earthquake warning systems in seismic-prone areas by investigating the data of different services, such as GEE, Giovanni and various other global satellite platforms services, such as Swarm. Finally, the path toward earthquake prediction is still long, and the goal is far, but the present results support the idea that this challenging goal could be achieved in the future.

Keywords: earthquake precursor; swarm satellite data; google earth engine; fuzzy inference system

Citation: Akhoondzadeh, M.; Marchetti, D. Study of the Preparation Phase of Turkey's Powerful Earthquake (6 February 2023) by a Geophysical Multi-Parametric Fuzzy Inference System. *Remote Sens.* **2023**, *15*, 2224. https://doi.org/10.3390/rs15092224

Academic Editor: Salvatore Stramondo

Received: 18 March 2023
Revised: 13 April 2023
Accepted: 21 April 2023
Published: 22 April 2023

1. Introduction

Strong earthquakes could be one of the heaviest and most catastrophic events among natural hazards, causing many victims and material-economic losses [1]. In spite of all the research done in the field of earthquakes, so far, no reliable scientific articles have been reported about the success in predicting the epicenter, origin time and (minimum) magnitude of multiple earthquakes with low uncertainty [2].

Satellite data are a very promising and suitable tool for studying various types of possible pre-earthquake anomalies due to the wide coverage, timeliness and lower costs compared to field data. Some of these anomalies could be good candidates as earthquake precursors. A precursor is an alteration of some chemical or physical properties of the lithosphere, atmosphere and ionosphere induced by the preparation phase of an earthquake. Consequently, any variations in geophysical layers could be potentially discussed as a precursor candidate. Despite this, it is important to note that not all variations before an earthquake are precursors, and specific studies have attempted to address this problem, for example, by statistical analysis [3–8].

These studies statistically demonstrated that ultra-low frequency (ULF) electromagnetic ground emissions, thermal infrared anomalies from satellites and ionospheric disturbances in the magnetic field and electron density are statistically recorded before medium–large earthquakes (M4+, M5.5+ or larger magnitude depending on the specific study). With the launch of a large number of remote sensing earth observation satellites, the wide variety and availability of data, the size and data processing time increased exponentially. The new cloud satellite data storage and data processing services, such as Google Earth Engine (GEE), provide a suitable platform for elaborating and obtaining results faster that, before, were not even possible in some cases [9].

On the other hand, with the advances made in human-controlled approaches and supervised or unsupervised machine-learning ones (i.e., artificial intelligence), the algorithms to detect possible pre-earthquake phenomena reduced the uncertainty in the field [10–13]. As a result, the number of false alarms in early warning systems can be reduced by using the multi-parameters analysis [14]. The reliability of this approach is supported by several case studies of multiple magnitudes analyses using a multiparametric and multilayer approach (e.g., M6.7 Lushan (China) 2013 [15], M7.8 Gorkha (Nepal) 2015 [16–18], M7.8 Muisne (Ecuador) 2016 [19], M6.5 Norcia (Italy) 2016 [20], M7.5 Palu (Indonesia) 2018 [21], M7.6 Papua New Guinea 2019 [22] and M7.2 Kermandec Islands (New Zealand) 2019 [23]). This study attempts to provide a basis for creating earthquake warning systems in highly seismic active areas by using the capabilities of the mentioned processing platforms.

Turkey–Syria Earthquake 2023

Based on the earthquake catalogue of the United States Geological Survey (USGS) website, on 6 February 2023, at 1:17:34 UT (about 4:15 a.m. local time), a striking earthquake of moment magnitude M_w = 7.8 occurred close to the border between Turkey (Türkiye) and Syria with the following hypocentral localization from USGS (https://earthquake.usgs.gov/earthquakes/eventpage/us6000jllz/executive, last access, 13 March 2023) (37.22° N, 37.02° E, 10.00 km depth). Due to the large magnitude of the event, a huge seismic sequence of aftershocks started and could continue for months or even years. In particular, but later, this was followed by a magnitude M_w = 6.7 aftershock that occurred 11 min after and was located at almost the same hypocenter.

At present (2nd March 2023), a moment magnitude M_w = 7.5 earthquake is the largest recorded aftershock localized 95 km to the north on a perpendicular fault. The relationship between M7.8 and M7.5 is debated in the seismological community. Considering that the two earthquakes are located on different faults, some researchers considered them as two mainshocks, but determine such a detail is out of the scope of this paper, as we regard all the events as a one geophysical event. Table 1 indicates the principal characteristics of the main seismic events from 1 September 2022 to 17 February 2023 around the epicenter.

Table 1. The principal parameters (hypocenter localization, magnitude and focal mechanism) of the principal seismic events ($M_W \geq 4.1$) around the epicenter (data retrieved from USGS, http://earthquake.usgs.gov/ (accessed on 26 February 2023)). Among the different available magnitudes, we selected the one more reliable and closer to a correct estimation of the released energy.

Time (UTC)	Latitude [°N]	Longitude [°E]	Depth [km]	Magnitude	Magnitude Type	Focal Mechanism
11 October 2022; 15:48:46	37.261	36.234	10.0	5.0	M_{ww}	Normal
18 December 2022; 18:13:09	36.392	36.491	10.0	4.6	M_{wr}	Strike-slip [1]
6 February 2023; 01:17:34	37.225	37.021	10.0	7.8	M_{ww}	Strike-slip
6 February 2023; 01:28:15	37.178	36.947	10.7	6.7	M_{ww}	Not Available (too close to the mainshock)
6 February 2023; 10:24:49	38.0234	37.203	10.0	7.5	M_{ww}	Strike-slip
6 February 2023; 10:26:48	38.030	37.964	20.1	6.0	M_b	Not Available
6 February 2023; 12:02:11	38.055	36.510	8.1	6.0	M_b	Not Available

[1] Data source for this information: Geofon seismic network (http://geofon.gfz-potsdam.de/eqinfo, accessed on 1 March 2023).

Figure 1 shows the locations of the M4.1+ earthquakes recorded starting from the 6 February 2023 M_w = 7.8 mainshock. We selected two smaller magnitude events recorded before the mainshock (called foreshock in the map) and very close or on the interested fault of these larger events. Despite these two events, no other significant foreshock has been recorded.

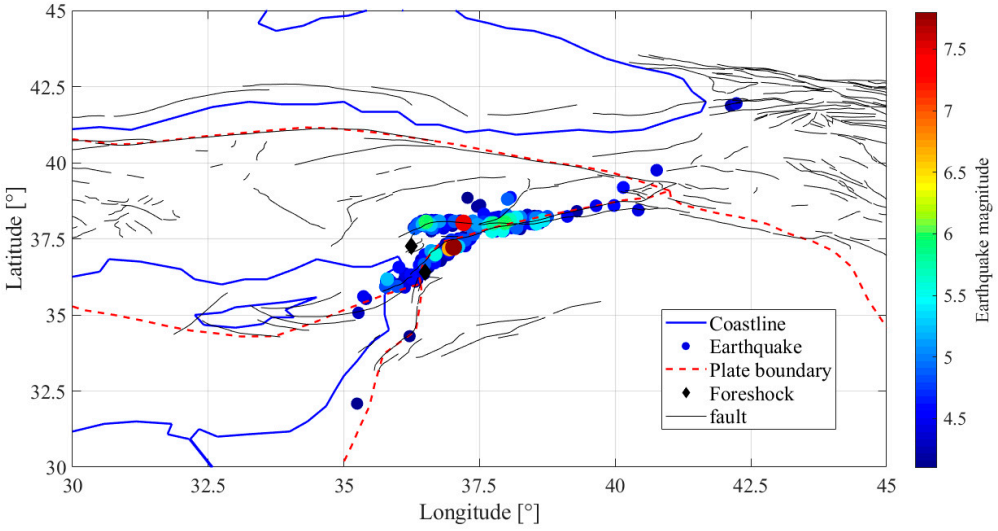

Figure 1. Map of the location of the recorded earthquakes by USGS with magnitude $M \geq 4.1$ from 6 until 17 February 2023. The plate boundaries are shown as red dashed lines and the two foreshocks reported in Table 1 as black diamonds. Faults were retrieved from the European Fault-Source Model 2020 (EFSM20) [24].

Both the largest earthquakes are a result of strike-slip transcurrance of two (or better three: Anatolian, Arabian and African) plates among an almost vertical fault plane.

2. Observations

Table 2 presents the 52 analyzed time series considered for the Turkey–Syria earthquake in order to search for possible pre-earthquake anomalies. These time series data were obtained via different data services, which are explained in more detail in the following.

Table 2. List of the analyzed time series before the Turkey 2023 earthquake (D: day, N: night, Ne: electron density, Te: electron temperature, AOD: aerosol optical depth and CO: carbon monoxide).

Parameters			Anomalous Days
Layer	**Satellite**	**Parameter**	
Ionosphere (plasma parameters)	Swarm A	Ne (D&N)	−8 to −1 (D), −2, −4 (N)
		Te (D&N)	—
	Swarm B	Ne (D&N)	−9 to −1 (D), −5 to −1 (N)
		Te (D&N)	−1, −3 (D)
	Swarm C	Ne (D&N)	−8 to −1 (D), −1, −4 (N)
		Te (D&N)	−1, −3 (D)
	Swarm A–C	Ne (D&N)	−4, −9 (D), −7,−1 (N)
	Swarm A–C	Te (D&N)	−4 (D), −34 (N)
Ionosphere (magnetic field data)	Swarm A	MS (D&N)	—
		MVx (D&N)	−3, −6 (D)
		Mvy (D&N)	−5, −8 (N)
		MVz (D&N)	−1, −8 (D), −8 (N)
	Swarm B	MS (D&N)	−5 (N)
		MVx (D&N)	−1, −3 (D)
		Mvy (D&N)	−3, −5 (D), −5, −33 (N)
		MVz (D&N)	−5 (N)
	Swarm C	MS (D&N)	—
		MVx (D&N)	−3, −6 (D)
		Mvy (D&N)	−5, −7, −8, −33 (N)
		MVz (D&N)	−4 (D),−1, −8 (N)
Atmosphere	GEE	Water vapor	−10
		Ozone	−7 to +1
	Giovanni	Methane (D&N)	+4 (D), −3 (N)
		Ozone (D&N)	−8 to +1 (D), −7 (N)
		CO (D&N)	−8 to +2 (D), −8, −9 (N)
		AOD	−9
	GEE	Surface temperature	−19 to −12
Lithosphere	USGS EQ catalogue	Daily number of EQ	−8
		Max EQ Magnitude	−75
Number of time series (D&N) 52			

2.1. Atmospheric Data

In this section, the atmospheric data are analyzed by means of time series investigation in Section 2.1.1 and by employing maps of each anomalous day depicted from the first analysis in Section 2.1.2.

2.1.1. Time Series Investigation of Atmospheric Data

This study used two modern platforms based on archiving and processing cloud data to analyze atmospheric data. The first is the Google Earth Engine (GEE) tool (https://earthengine.google.com/, accessed on 20 February 2023), and the second one is the Giovanni data service (http://giovanni.sci.gsfc.nasa.gov/giovanni/, accessed on 20 February 2023) from NASA. The details of the atmospheric data used in this study are given in Table 3. The area used for the atmospheric investigation is shown in Figure 2, together with the epicenter. It should be noted that this study area (the red polygon) was selected along the main fault, and the reported aftershocks are mapped in Figure 1.

Table 3. The details of the atmospheric data used in this study.

Variable	Source		Spatial Resolution
Water vapor	GEE	NCEP_RE	1 degree
Ozone		TOMS/MERGED	1 degree
Surface temperature		NOAA/VIIRS	1 km
Methane, mole fraction in air, ascending	Giovanni	Aqua/AIRS	1 degree
Ozone, total column, ascending		Aqua/AIRS	1 degree
Carbon monoxide, mole fraction in air, ascending		Aqua/AIRS	1 degree
Aerosol absorption optical depth 500 nm (dark target)		MODIS-Aqua	1 degree

Figure 2. The geographic location of the 2023 Turkey earthquake. The black star represents the epicenters and red polygon shows the analyzed region of interest (map produced by https://earthengine.google.com/, accessed on 7 April 2023).

The time series of water vapor, ozone and surface temperature variations in the occasion of the Turkey–Syria earthquake (6 February 2023) from 1 September 2022 to 17 February 2023, retrieved from GEE platform, are illustrated in Figure 3. The daily average of these observations in the red polygon shown in Figure 2 from 1 September 2022 to 17 February 2023 was calculated using the GEE computing platform to obtain such a time series. The horizontal axis, i.e., the time, was calculated with respect to the days of the earthquake occurrence, indicated by a black dashed vertical line. The median, upper and lower boundaries (i.e., the anomaly detection thresholds) are reported as blue and green lines, respectively. These thresholds were pre-defined as, where "M" is the median and "Iqr" is the interquartile range value of the distribution of the observations. The choice of a median and interquartile method was selected to address the non-gaussian distribution of original data. This technique has also been proposed by Pulinets et al. [25] and Liu et al. [26].

A striking water vapor anomaly 10 days prior to the mainshock is indicated by a black arrow in Figure 3a. It exceeds the upper boundary by a percentage of 24.13% of the typical value.

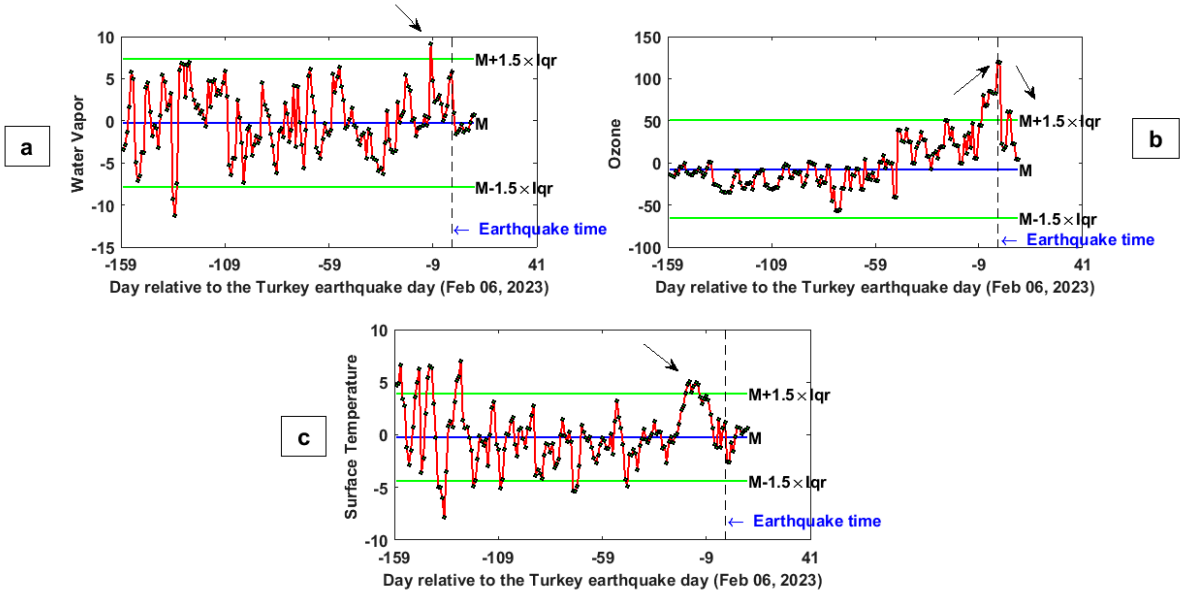

Figure 3. Time series of (**a**) water vapor, (**b**) ozone and (**c**) surface temperature variations for the Turkey earthquake (6 February 2023) from 1 September 2022 to 17 February 2023, retrieved from the GEE platform.

Clear ozone anomalies are evident in Figure 3b from 7 days before to 1 day after the earthquake. This parameter reached the maximum anomaly with a percentage value of 53.88% above the upper threshold 1 day prior to the event (the black arrow in panel b). Furthermore, it is outstanding to observe that, in the first 100 days, the time series seems to have standard oscillations with a flat trend, after, i.e., from about 55 days prior to the main-shock, it started to increase and then decreased after the event. The ozone anomalies before the earthquakes are phenomena documented in the literature both from the theoretical point of view of the lithosphere atmosphere and ionosphere coupling models and empirical observations [27–30]. It can be explained considering that the stress gradually increases in the inter-seismic (preparation) phase of an earthquake as long as the fault is recharging after the previous important event. This phenomenon is the source of several possible effects, such as the fluid–gas migration, gases or even the release of radon and positive holes from the ground [31–35]. This leads to the possible observation of anomalous atmospheric concentrations (such as the one identified in Figure 3) and electrical precursory phenomena. In particular, the underground accumulation of stress and fluid migration could result in the release of gases at the Earth's surface, among them methane, water vapor, hydrogen, nitrogen and CO, consequently affecting the ozone concentration in the atmosphere [28,36].

Figure 3c shows that the surface temperature parameter exceeds the upper bounds 19 to 12 days in advance with respect to the earthquake, as marked by the black arrow in panel c. Wide literature from different researchers has provided empirical pieces of evidence and theoretical support for thermal anomalies, which may be induced by the preparation phase of earthquakes [37–39]. Russia, China and Japan even attempted to operatively apply of thermal anomalies for prediction purposes. In particular, thermal anomalies have been reported before earthquakes in central Asia, Turkey, Iran and other areas [37,40,41].

It should be noted that the thermal anomalies could be caused by other phenomena, especially severe atmospheric perturbations or extreme weather events due, for example, on overheating of Sea or land in consequence of lack of standard precipitation induced by climate change. In the case of an earthquake, the thermal anomaly could be due to the underground increase of the stress at the seismic source depth and possible alterations of the underground properties. Qiang [42], Di Luccio et al. [33], Saradjian and Akhoondzadeh [41] and Chiodini et al. [43] proposed and measured that, in the preparation phase of earthquakes, greenhouse gases, such as CO_2 and methane, could be emitted due to deep fluid

migration and emitted at the Earth's surface. The emanation of such gases could even alter the atmosphere's and ionosphere's electromagnetic properties [44].

Figures 4 and 5 show the time series of methane, ozone, carbon monoxide and the aerosol optical depth (AOD) variations for the Turkey earthquake, from 01 November 2022 to 17 February 2023, retrieved from the Giovanni data service. It should be noted that some gaps are present during these time series due to a lack of satellite coverage or cloud coverage that did not permit extrapolating the atmospheric composition.

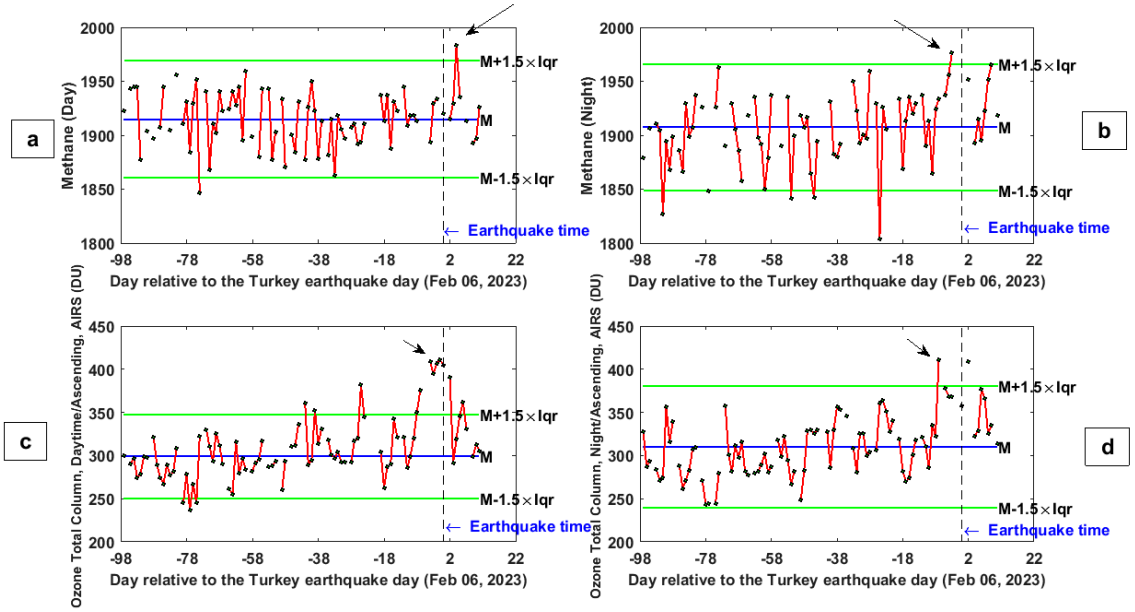

Figure 4. Time series variations of (**a**,**b**) methane at day and night, respectively, and (**c**,**d**) ozone at day and night, respectively, for the Turkey earthquake (6 February 2023) from 1 November 2022 to 17 February 2023, deduced from the Giovanni data service.

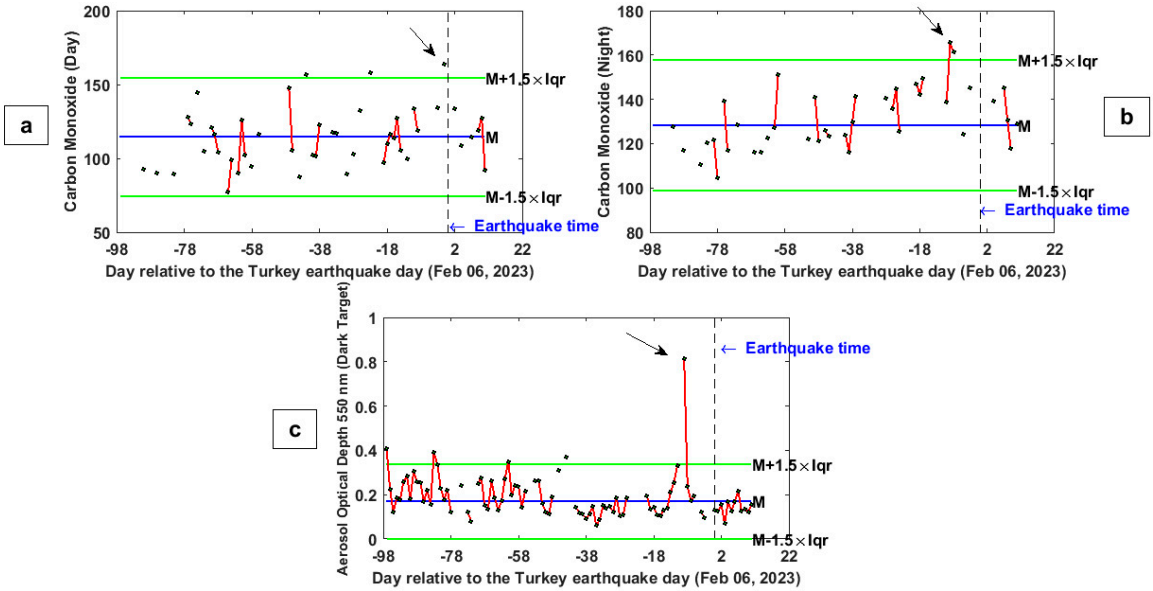

Figure 5. Time series variations of (**a**,**b**) carbon monoxide at day and night, respectively, and (**c**) aerosol optical depth for the Turkey earthquake (6 February 2023) from 1 November 2022 to 17 February 2023, deduced from the Giovanni data service.

Figure 4a indicates a clear daytime methane anomaly with the values of 26.49%, 4 days after the earthquake (the black arrow in panel a). It could be due to some oil pipe

leakage and other damages caused by these earthquakes as reported by some newspapers (e.g., https://www.offshore-technology.com/news/turkey-earthquake-damages-gas-pipeline/, last access 8 April 2023). However, the nighttime variation trend of the methane time series shows a striking anomaly 3 days before the event exceeding the upper bound with a percentage value of 17.46% (the black arrow in panel b).

To confirm the results of ozone variations deduced from GEE platform, here, the same parameter is analyzed via a different platform and data service. The main difference is that, here, the methane is directly retrieved from satellite observations, while, before, an atmospheric chemical model was applied in data pre-processing. Panels c and d in Figure 4 show the ozone total column parameter measured by AIRS satellite during day and night, respectively.

Clear anomalies were seen from 8 days before to 1 day after the Turkey–Syria earthquake at daytime ozone time series variations. This parameter reached the maximum value of 128.10%, 1 day before the event. The nighttime ozone variations indicate a striking anomaly, 7 days before the Turkey–Syria earthquake, reaching a percentage of 43.11% above the threshold.

The variations of carbon monoxide as another important possible pre-earthquake atmospheric gas [45] show clear anomalies from 8 days before to 2 days after the event during daytime with a maximum value of 128.10% 1 day before the earthquake (Figure 5a). Figure 5b illustrates that carbon monoxide during the nighttime exceeds the upper boundary 8 and 9 days before the event with values of 12.22% and 27.21%, respectively. Carbon monoxide could also be related to carbon dioxide, which is known to be possibly related to seismic activity. However, some works of literature found it more in a tectonically extensional context [32,46].

Figure 5c clearly shows striking aerosol anomalies 9 days prior to the Turkey–Syria earthquake. In particular, the AOD parameter overpassed the upper boundary of the extreme value of 281.41%. Such an extreme value is unlikely to be caused by the incoming earthquake as confirmed by a specific back-tracing of the source of this anomaly provided in Appendix B. After the earthquake, the aerosol value came back slightly below the median trend. This could be unexpected as the dust was transferred into the atmosphere due to the collapse of buildings. The data source used to calculate such time series has too low of a spatial resolution to catch such small local variations that vanish when mediated on a large pixel. In fact, the study of remote sensing assessment of damaged buildings is made with much higher spatial resolution data (e.g., Romaniello et al. [47] investigated the damages of M_w = 7.0 2010 Haiti earthquake with 30 m resolution remote sensing data).

The increase of aerosol in the atmosphere was discussed by Pulinets and Ouzounov [48] as a result of physical and chemical processes induced by the release of radon. We noted that the theory of Freund [34,49], which propose the release of positive charges (or p-holes) instead of radon, could induce the same atmospheric (and ionospheric) chain predicted by Pulinets and Ouzounov [48]. In detail, the last one theorizes a "domino" effect based on the hydration of suspended particles that could also increase the aerosol concentration in the atmosphere until the formation of pre-earthquake clouds.

An increase of aerosol before several earthquakes has also been reported with an almost perfect chain of lithosphere-atmosphere and ionosphere anomalies from 2.5 until one weeks before M_w = 6.7 Lushan (China) earthquake [15], and in the case of the M_w = 7.5 Indonesia 2018 earthquake with synchronous electromagnetic ionospheric disturbances [21]. The possibility that the formation of aerosol and air ionization could be the source of seismo-ionospheric anomalies is supported by the theories of Pulinet and Ouzounov [25,48,50], and the results of this paper are compatible with such a theoretical framework.

2.1.2. Map Investigation of the Anomalous Atmospheric Days

In this section, we present the maps of the anomalous days extracted from the previous section, i.e., by time series analysis. For each parameter, we extract one map of a day above the threshold, i.e., anomalous. The map of the parameter can help to discriminate whether

the anomaly is spatially related to the fault system (i.e., the plate boundary) or can be only superposed in the area. Figure 6 shows the map of aerosol on 18 January 2023, Temperature on 25 January 2023, specific humidity on 27 January 2023, carbon monoxide (CO) on 29 January 2023, total column ozone on 30 January 2023 and, finally, methane mixing ratio on 3 February 2023.

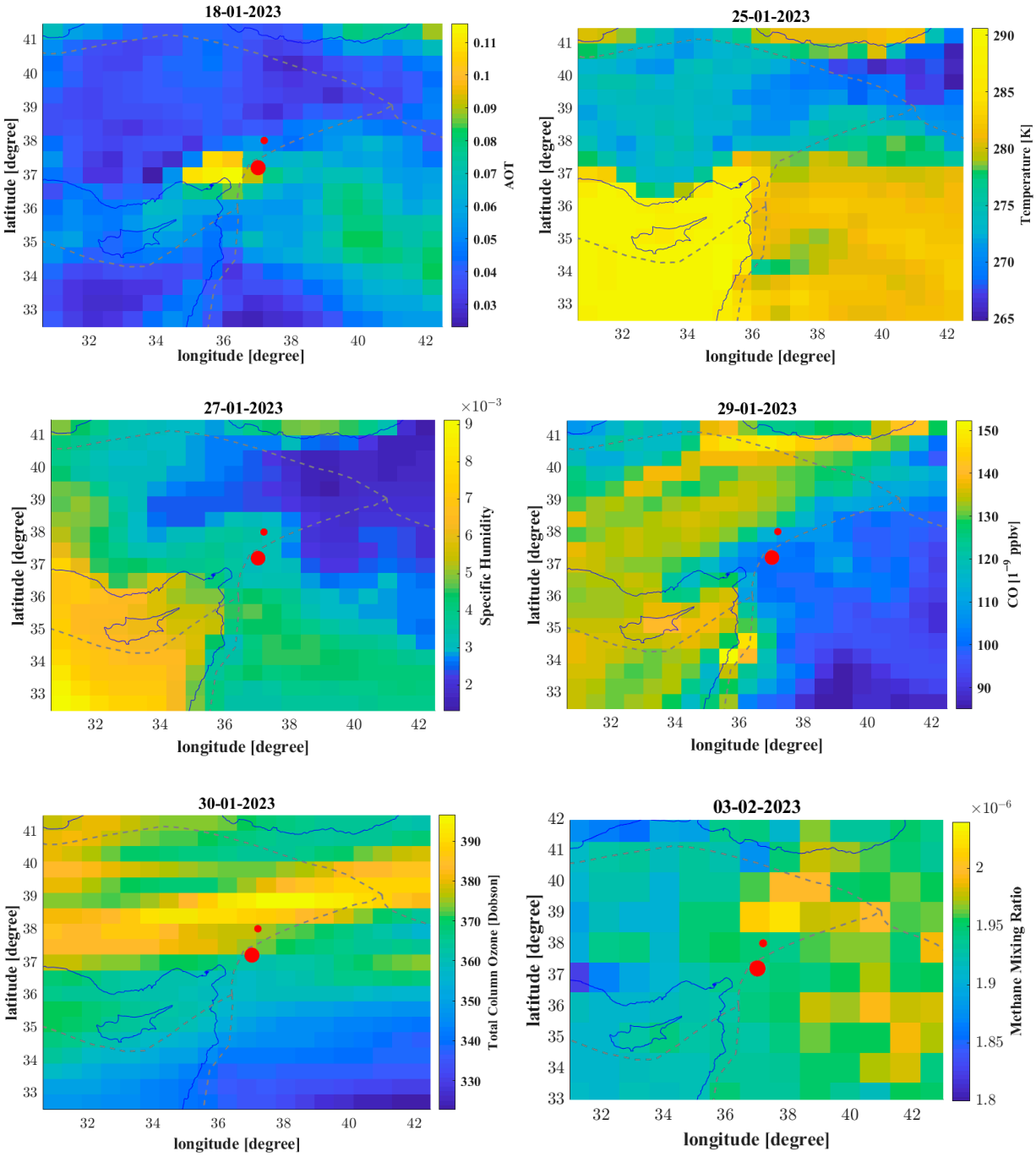

Figure 6. Maps of the anomalies identified by the time series. The epicenters of the two main earthquakes that occurred on 6 February 2023, of magnitude 7.8 and 7.5, are shown with a red dot whose size is proportional to their magnitude. The grey dashed line is the plate boundary.

For methane data, as the AIRS instrument provides the mixing ratio over 24 vertical pressure levels, we selected the closer to the ground in order to select the value more representative of lithosphere status as done in the past for Ridgecrest 2019 and Papua New

Guinea 2019 earthquakes [22,51]. We decided to order the map in chronological order in order to depict also possible sequences of atmospheric anomalies in the atmosphere that can help to discriminate a specific eventual lithosphere atmosphere and ionosphere coupling model according to what has been done, for example, for La Palma 2021 volcano eruption [52] or for Lushan 2013 earthquake [15].

Looking in detail at the map, it is possible to note that the anomaly of the aerosol of 18 January 2023 is very close to the incoming earthquakes and so spatially highly compatible with the emission of gases from the active faults in preparation for the earthquake [53]. Similar considerations can be made for methane emission that were shown to be well spatial superposed with the plate boundary and, in particular, with the triple point of interaction of the three faults (Anatolia, Arabia and Africa plates).

The plate boundary and, in general, the fault is a natural channel where underground fluid and gases can be released on Earth's surface [54]. The ozone map still looks interesting because it shows an extended anomaly parallel to the fault of the incoming earthquake but shifted. Compared with the normal trend of ozone, which is normally depending on the latitude, it is outstanding that it shows a local trend instead, so it seems the source of this distribution of ozone may be regional.

However, further evidence of connection with the earthquake is required in future studies and combined with local geochemical monitoring instrumentation on the ground where available. Concerning the surface air temperature map on 25 January 2023 and specific humidity on 27 January 2023, they do not seem to be spatial related to the incoming earthquake suggesting maybe other phenomena, such as over warming of the Mediterranean Sea, that brought heat waves and humidity changes on the closer lands.

2.2. Ionospheric Parameters

To distinguish external disturbances with eventual seismo-ionospheric anomalies, we reported in Figure 7a,b the values of K_p, a_p and Dst geomagnetic indices from 1 September 2022 to 17 February 2023. Each index is more representative of some characteristics of the status of the geomagnetic field. In particular, a_p and K_p are global indices measured from several geomagnetic observatories at different latitudes in linear and logarithm scales. The Dst index is measured by four geomagnetic observatories around the dip equator. In the impact of a geomagnetic storm, its values become negative and could reach some hundreds of nT of intensity in function of the strength of the same perturbation.

Consequently, high a_p or K_p and/or low values of Dst could indicate an external geomagnetic activity. We would exclude this perturbed time in the anomalies exploitation because their source is more likely to be external. The selected quiet time for each index was depicted by two colors (binary representation) in order to visualize the quiet geomagnetic time in green directly.

The horizontal axis represents the days relative to 6 February 2023, i.e., the Turkey–Syria earthquake day. In addition to geomagnetic conditions, we monitored also the solar activity looking for the trend of the F10.7 index plotted in Figure 7c. It is important to take in mind that the conditions during the investigated months are within a rising of solar activity of the 25th cycle, which is recording an activity stronger than the predicted one (https://www.swpc.noaa.gov/products/solar-cycle-progression, accessed on 2 March 2023) both for Sunspot number and F10.7.

The choice of the conditions to define calm or perturbed geomagnetic periods was based on our previous experience in analyzing other strong earthquakes in the world [14,19,22,55–57].

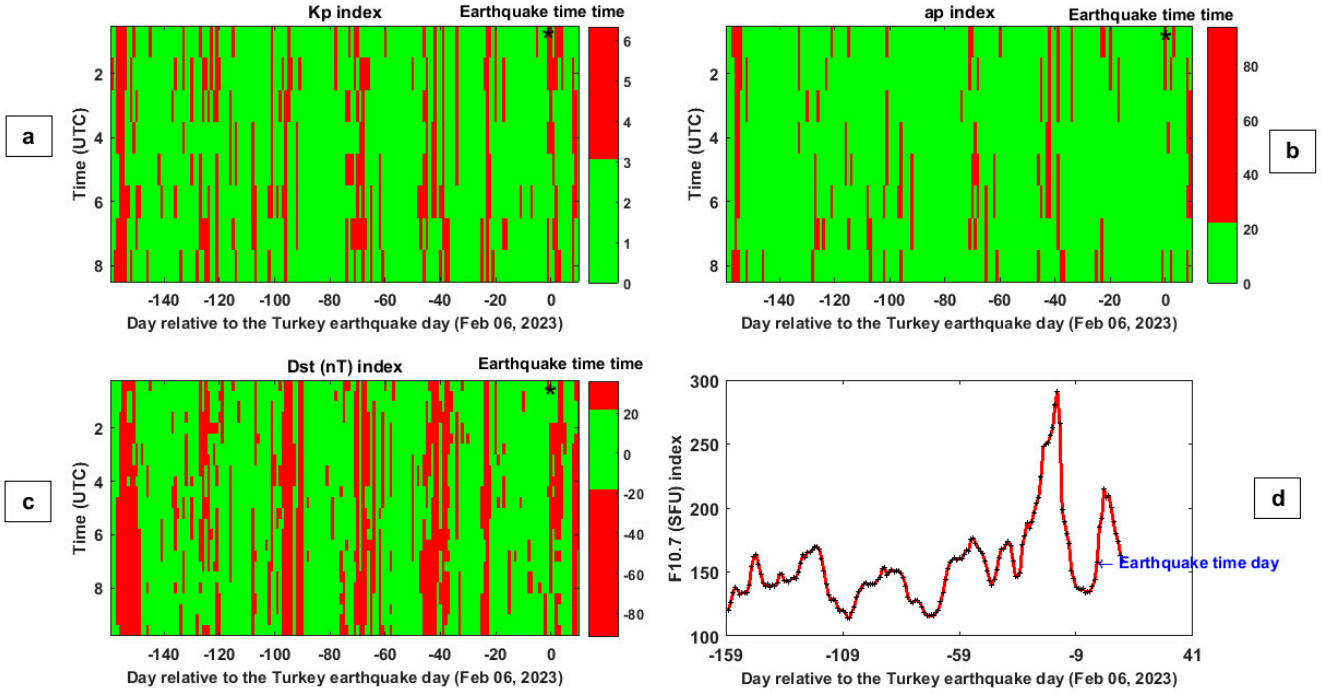

Figure 7. (**a**–**d**) variations of K_p, a_p, Dst, and F10.7 geomagnetic indices, respectively, during the period from 1 September 2022 to 17 February 2023. An asterisk "*" indicates the earthquake origin time of Turkey–Syria (6 February 2023). The abscissa represents the days relative to the earthquake day. The values of the geomagnetic indices are provided as binary, i.e., red for not-quiet magnetic times and green for quiet magnetic times according to each index.

In particular, $K_p < 3$ nT, $a_p < 20$ nT, $|\mathrm{Dst}| \leq 20$ nT, and F10.7 <180 SFU (Solar Flux Unit) are our constraints to select geomagnetic and solar quiet conditions. Notably, the earthquake occurred about 10 days after a very strong peak of solar activity, as the F10.7 reached about 300 SFU. The possible trigger of high solar-geomagnetic activity on powerful earthquakes, by inserting a large number of energetic particles in Earth's environment, was supported by Marchitelli et al. [58]. Nevertheless, Akhoondzadeh and De Santis [59] found that the increase in seismicity after a large solar activity is not statistically significant. The scientific debate is still open, and in any case, this aspect is out of the scope of this paper.

In studies about pre-earthquake processes, normally, a research area possibly affected by the earthquake is considered. Here we use the circular area defined by Dobrovolsky et al. [60]'s and equal to $R = 10^{0.43M}$, (km), which increases exponentially with the magnitude M of the incoming earthquake. Only the sections of the satellite track inside this research area are taken into account to search for possible seismo-ionospheric pre-earthquake anomalies. Then, all track sections are divided into two groups: (1) day and (2) nighttime.

This is to take into account that the ionosphere is strongly influenced by solar irradiation. Consequently, its behavior is quite different at night and day. In the next data processing step, the median of the specific parameter was calculated, and the time series with upper and lower thresholds were estimated. Finally, a polynomial of degree 3 was fitted and subtracted in order to remove any residual trend possible due to seasonal variations of the plasma parameters.

The three Swarm satellite daytime electron density time series before and after the Turkey–Syria earthquake (black dashed vertical line) are reported in Figure 8. The median and thresholds (i.e., the upper and lower boundaries) are represented with blue and green horizontal lines, respectively. The 'P' letter (that stands for "perturbed") indicates days with high geomagnetic or solar activity. We underline that the thresholds to extract the anomalies were estimated only by using the quiet geomagnetic and solar days.

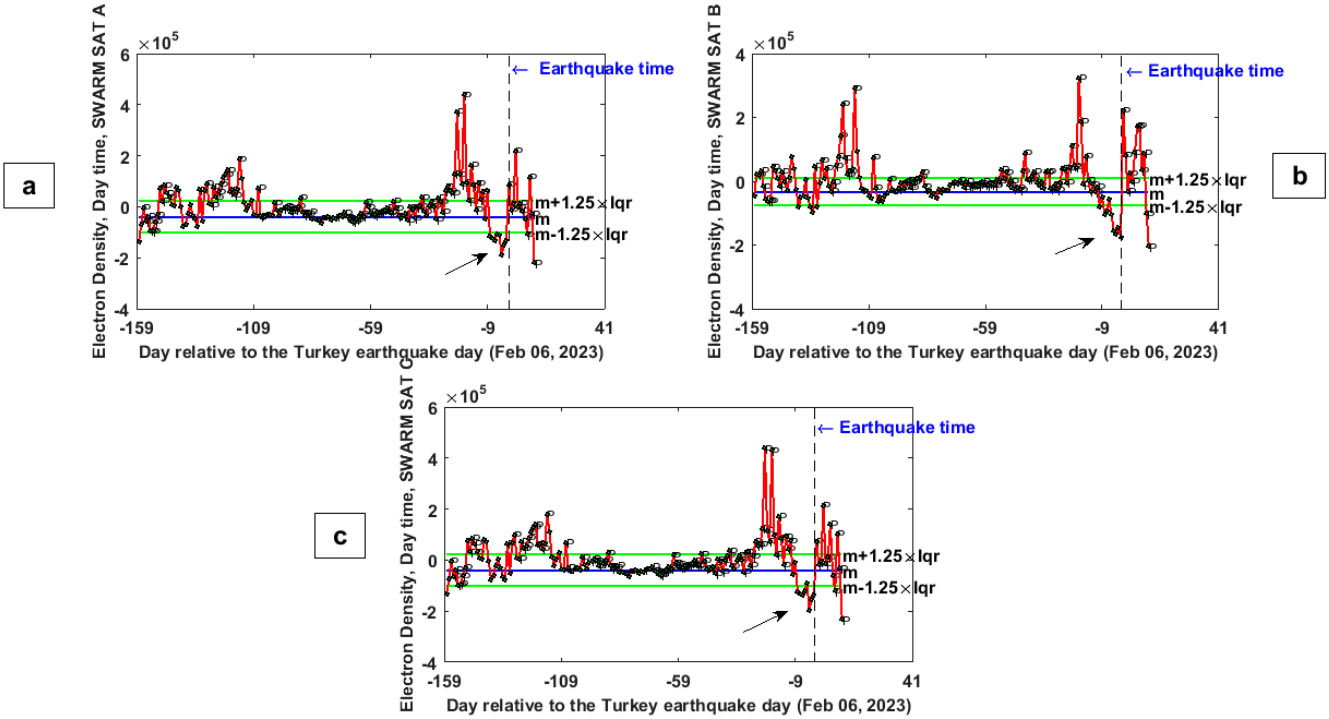

Figure 8. Results of Swarm (**a**–**c**) electron density data analysis for the Turkey–Syria earthquake (6 February 2023) from 1 September 2022 to 17 February 2023 at nighttime. Blue and green lines represent the median value and the selected thresholds to detect the anomalies. If a day experiences some geomagnetic perturbations, it is depicted with the letter "P" on the graph.

The panels (a, c) of Figure 8 clearly show striking Ne anomalies 3 days before the Turkey–Syria earthquake in the Swarm A and C measurements. The intensity of these anomalies was considerable: the parameter was lower 3 days before the event than the threshold with percentage values of 107% and 106% for Swarm A and C, respectively (the black arrows in panels a and c). Furthermore, it is worth mentioning that the time series of *Ne* variations measured by Swarm satellite B 1 day before the Turkey–Syria earthquake was lower than the boundary of a percentage value equal to 172%.

Considering the peculiarity of the Swarm constellation with the two satellites A and C flying in close the same-altitude orbits (separated by 1.4° longitude at the equator or less), it is possible to compare the electron density measured by the two platforms directly. Calculating such differences will allow detecting possible rapid ionospheric variations that we can evaluate and test as potential candidates as earthquake precursors. The time series of the electron density comparison between satellites A and C in day and night time are shown in Figure 9.

On 4 and 9 days before the Turkey–Syria earthquake, special values of the Ne difference between Swarm A and C were detected, exceeding the allowed boundaries with percentage values of 713% and 43.0%, respectively, during daytime. Figure 9b indicates that the time series of *dNe* exceeded the allowed boundaries 1 and 7 days prior to the Turkey–Syria earthquake with values of 69.5% and 85.9% during nighttime.

Such ionospheric anomalies are really interesting, but there could be two equally plausible geophysical explanations: (1) they were induced by the peak of solar activity that is depicted as only a few days before in Figure 7d even though this event seems to not have disturbed the geomagnetic environment (as the index remained low), but some solar wind particles could have impacted the ionosphere; (2) the increase in the ionospheric anomalies from 9 days to 1 day before the seismic event was caused by its preparation, also considering that the same time was found for the same magnitude earthquake occurred in Ecuador in 2016 [19,61].

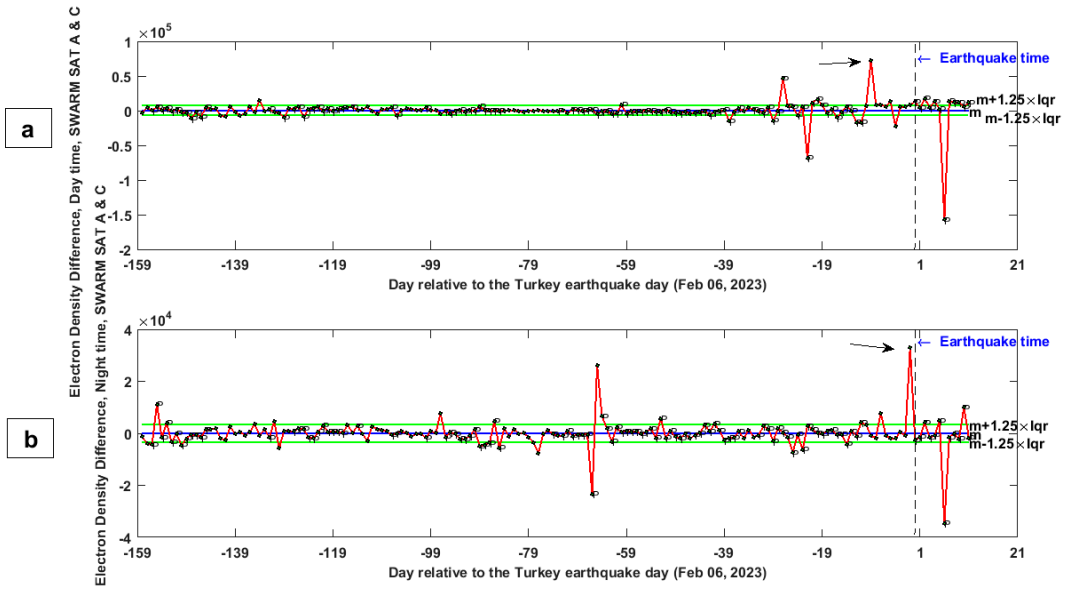

Figure 9. Results of Swarm A and C electron density differences for the Turkey–Syria earthquake (6 February 2023) from 1 September 2022 to 17 February 2023 in the daytime. Panels (**a**,**b**) represent day and night times, respectively. The geomagnetically "perturbed" days are highlighted by a "P".

In order to deeply investigate the ionosphere behavior prior to the seismic event, a track-by-track analysis was done. In particular, the daytime tracks of satellites A on an anomalous day (3 February 2023, i.e., 3 days before the Turkey–Syria earthquake) are shown in Figure 10a, depicting a couple of anomalies at geomagnetic latitudes of 25° N and 32° N inside the Dobrovolsky's research area. In the figure, the geographical elements, such as the epicenter, the projection of the satellite track and Dobrovolsky's circle, are plotted in the map in panel a. The residual difference on the specific track between the observed electron density/temperature and a 12-degree fitted polynomial are plotted in panels (b,c).

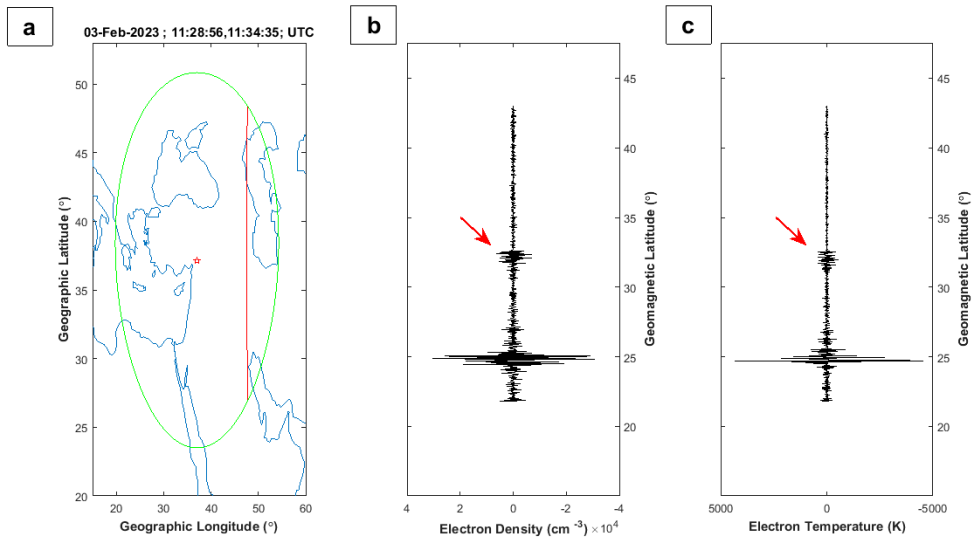

Figure 10. Results of Swarm A track analysis for the Turkey earthquake (6 February 2023) on 3 February 2023, 3 days before the earthquake. (**a**) The earthquake epicenter, the track and Dobrovolsky's area are shown as a red asterisk, a red line and a green circle, respectively. The track passed Dobrovolsky's area between 11:28:56 and 11:34:35 UTC. The horizontal and vertical axes represent the geographic longitude and latitude. (**b**,**c**) show the differences between the measured electron density and temperature time series and a fitted polynomial of degree 12 along this track. The vertical axis represents the geomagnetic latitude.

Considering that the ionospheric structures are typical of a specific geomagnetic latitude, we reported this one on the vertical axis instead of the geographical latitude. The tracks present two anomalies: one at the same latitude as the incoming earthquake (the red arrows in Figure 10), which we propose as a possible seismo-induced candidate, and another anomaly that is placed in the transition between land and Persian Gulf Sea and this land/sea variation could be the source. We cannot exclude that some underground fluids could even migrate and release close to the local place where the anomaly was detected due to the special geological features of the lithosphere, but this last hypothesis is weak.

To further investigate the ionosphere, searching for eventual magnetic field anomalies, the scalar and vector magnetometer observations were investigated. The algorithm first subtracts the IGRF (International Geomagnetic Reference Field [62]) model from the Swarm satellite data acquired with good-quality flags. Secondly, all the residual values for nighttime and daytime were considered, and their median was computed. Finally, the time series from 1 September 2022 to 17 February 2023 was plotted after subtracting a 3-degree polynomial to remove further seasonal variations of the geomagnetic field. The anomalies were defined by checking any eventual residual value that overpasses the threshold selected a priori. The specific observed parameter is considered anomalous only if measured in geomagnetically and solar quiet conditions ($K_p < 3$ nT, $a_p < 20$ nT, $|Dst| \leq 20$ nT and F10.7 < 180 SFU) following the approach already applied in our previous works [19,22,55–57].

Results of vector Y magnetic field component during night time from Swarm B and C data analysis from 01 September 2022 to 17 February 2023 are shown in Figures 11 and 12, respectively. As in the previous ionospheric time series, the perturbed days for geomagnetic or solar activity are marked with a "P". We noted that a couple of days of Swarm B are anomalous for the magnetic field Y component, i.e., their value exceeded the boundaries of the time series 5 and 33 days before the earthquake (Figure 11). This parameter also shows unusual variations between 3 and 7 days before and 33 days preceding the seismic event in the time series extrapolated from Swarm C (Figure 12).

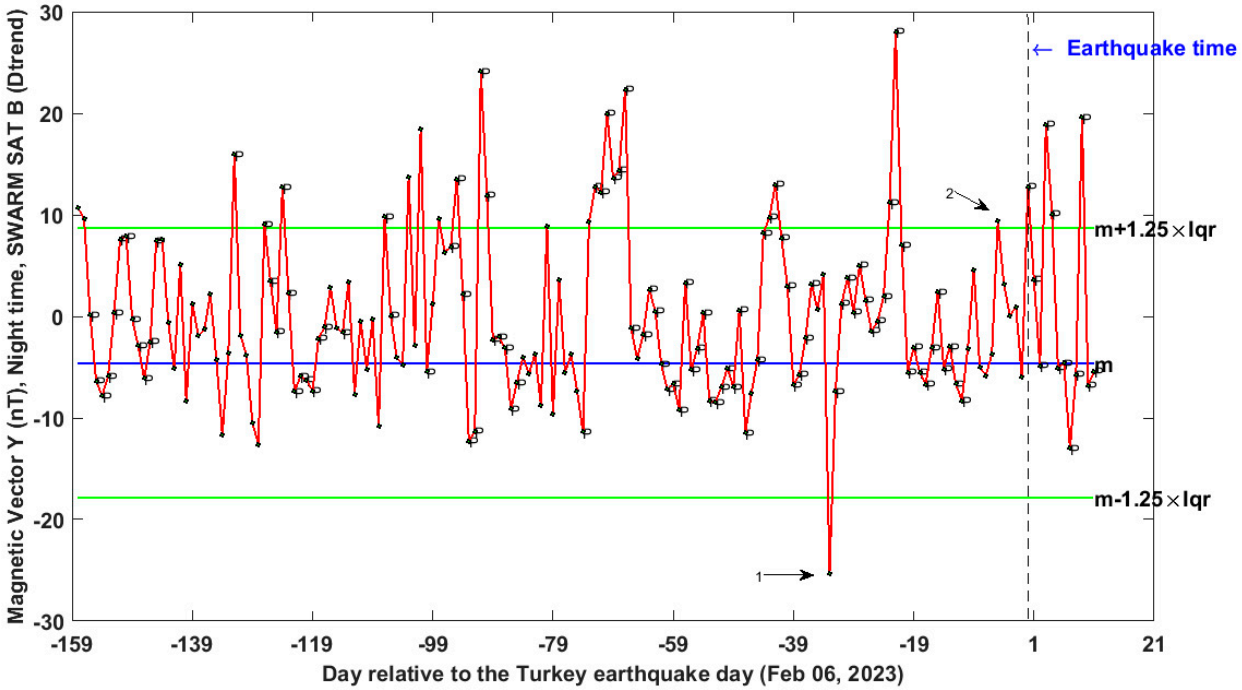

Figure 11. Results of Swarm B vector Y magnetic field data analysis for the Turkey–Syria earthquake (6 February 2023) from 1 September 2022 to 17 February 2023. The black arrows 1 and 2 indicate the potentially pre-seismic anomalies.

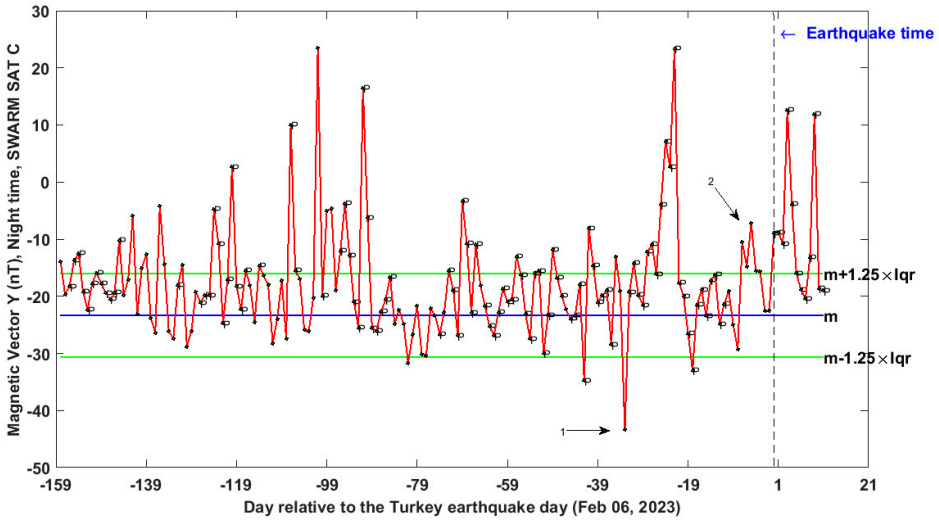

Figure 12. Results of Swarm C vector Y magnetic field data analysis for the Turkey–Syria earthquake (6 February 2023) from 1 September 2022 to 17 February 2023. The black arrows 1 and 2 indicate the potentially pre-seismic anomalies.

Figure 13 reported an anomalous track in quiet geomagnetic conditions of Swarm B preceded by 3 days Turkey–Syria earthquake (6 February 2023). Panel a depicts the same geographical elements of panela a in Figure 10. During the shown track, the satellite crossed Dobrovolsky's area from 22:59:17 to 23:04:46 UTC. The panels b, c, d and e show the residual values computed as derivatives of the observations. The red arrows in Figure 13 indicate a clear anomaly that appears in all vectorial components of the geomagnetic field but not in the scalar intensity. This means that this alteration is a rotation of the magnetic field direction but not of its intensity, possibly caused by the preparation phase of the Turkey–Syria earthquake as suggested but the same latitude with respect to the epicenter one.

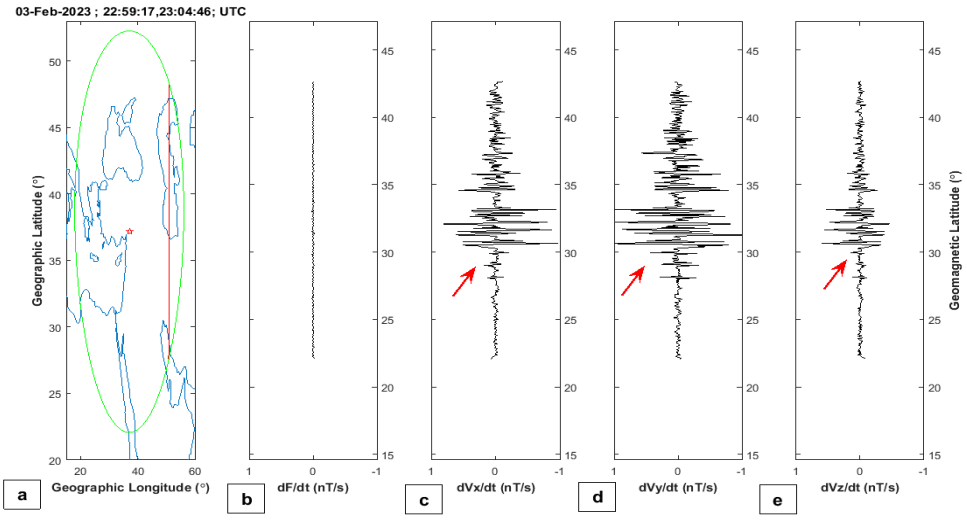

Figure 13. Results of Swarm B track analysis for the Turkey–Syria earthquake (6 February 2023) 3 days before the earthquake. The earthquake epicenter, the track and Dobrovolsky's area are shown as a red star, a red line and a green circle, respectively, in panel (**a**). The track passed Dobrovolsky's area between 22:59:17 and 23:04:46 UTC. The horizontal and vertical axes represent the geographic longitude and latitude. The subfigures (**b**–**e**) show the residuals of the derivatives of the measured values of scalar intensity and magnetic vectors (X, Y, Z) fields, respectively. The vertical axis represents the geomagnetic latitude. This analysis is performed inside the region's minimum and maximum Dobrovolsky latitudes.

3. Prediction of Earthquake Magnitude Using FIS

In this section, we try to apply the system based on fuzzy logic, which we previously developed for five different earthquakes to predict the incoming magnitude based on the lithosphere, atmosphere and ionosphere time series anomalies [14]. A Fuzzy Inference System (FIS) is a system that attempts to use a continuous logic, instead of a binary Boolean one, to predict an output quantity by another input parameter. The decision process of FIS attempts to imitate the human decision way by using this fuzzy logic approach (i.e., constructing a series of IF-THEN conditions) [63]. We already proposed a new system based on Mamdani [64] FIS to estimate the earthquake magnitude, whose details can be found in [14].

Applying FIS to the Turkey–Syria earthquake of 6 February 2023, we obtained the result reported in Figure 14. In particular, panel a summarise the daily number of anomalies (green bar) that is the input of FIS; panel (b) reports the output of FIS, which is the daily predicted earthquake magnitude (red bar), and panel c shows the observed maximum daily magnitude from 1 September 2022 to 17 February 2023. It is outstanding to note that as the earthquake was approaching, a larger concentration of anomalies was visible (see panel a in Figure 14a). FIS predicts a magnitude M = 7.0 earthquake 9 days before the earthquake (Figure 14b) and a magnitude M = 7.2 earthquake 1 day before the event. The real recorded earthquake magnitude was M_w = 7.8. These results further confirm the one obtained in the previous paper and support the idea to use the 3 geo-layers (lithosphere atmosphere and ionosphere) to monitor the earthquakes in quasi-real time as proposed by Marchetti et al. [65].

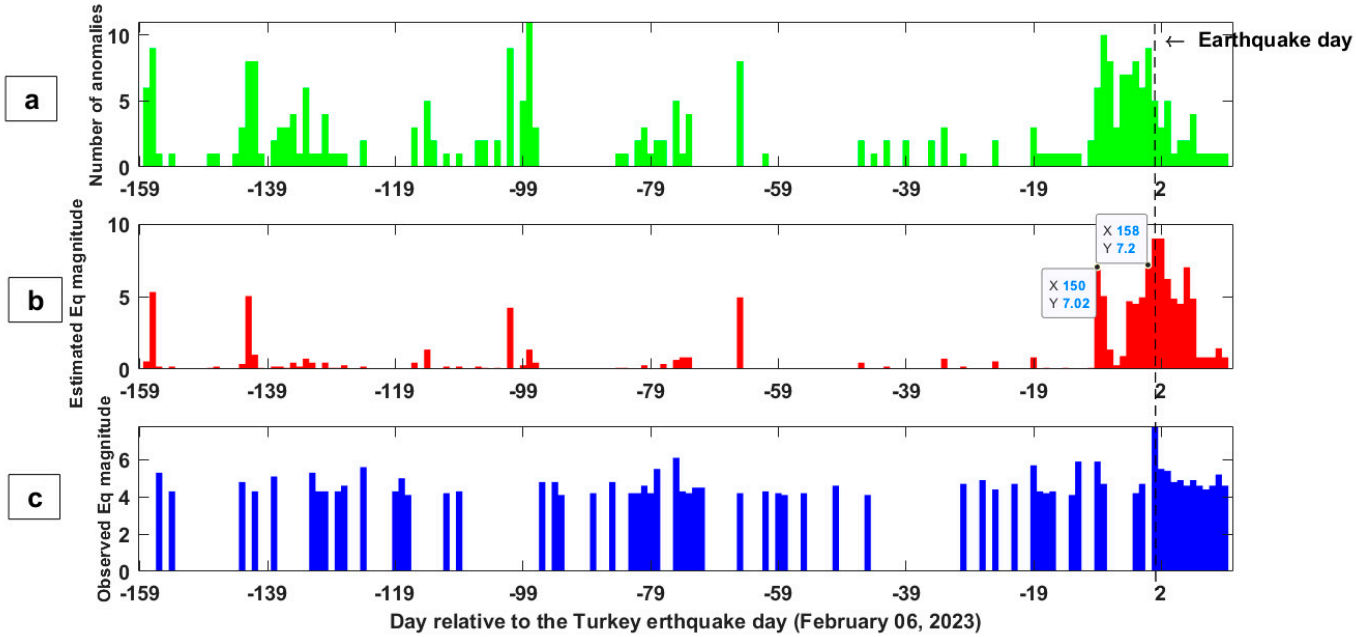

Figure 14. (**a**) Variation in the number of anomalies (green bars), (**b**) variation in the predicted earthquake magnitude (red bars) and (**c**) the observed earthquake magnitudes (blue bars) around the Turkey–Syria earthquake (6 February 2023) from 1 September 2022 to 17 February 2023. In all panels, the *x*-axis represents the day relative to the earthquake day indicated as a vertical dotted line.

4. Discussion

In this paper, several anomalies from the lithosphere atmosphere and ionosphere were extracted. Especially the atmospheric anomalies are the most reliable in this work. Still, it is not possible to exclude a weather alteration induced by the strong solar activity recorded a few days before (see Figure 7d), and climate, magnetic field and solar activity are all probably related as part of the same geodynamical system (e.g., [66]).

In the following, we would like to discuss the anomalies in the several geo-layers in a similar way done for the Italian seismic sequence 2017-2017 by Marchetti et al. [20], which identified a chain of processes that preceded the start of the seismic sequence or for Nepal M7.8 and M7.2 2015 earthquakes by Ouzounov et al. [16], which identified possible couplings between the different geo-layers with few days of delay or more recent work for Lushan 2013 earthquake by Zhang et al. [15], which identified different couplings explainable by specific LAIC models.

Figure 15 summarizes all the identified anomalies in this paper in a multi-geo-layer (lithosphere, atmosphere and ionosphere) view. For the lithosphere, two foreshocks were extracted in the investigated period, which occurred on the same fault or very close to the mainshock(s) of 6 February 2023 (M_w = 7.8 and M_w = 7.5). These events can even be considered as seismic precursors of the incoming earthquake, and we included the one that occurred on 18 December 2022 in Figure 15 and not the one on 11 October 2022 to not stretch too much on the time scale as we prefer to focus in the last months and weeks before the earthquake.

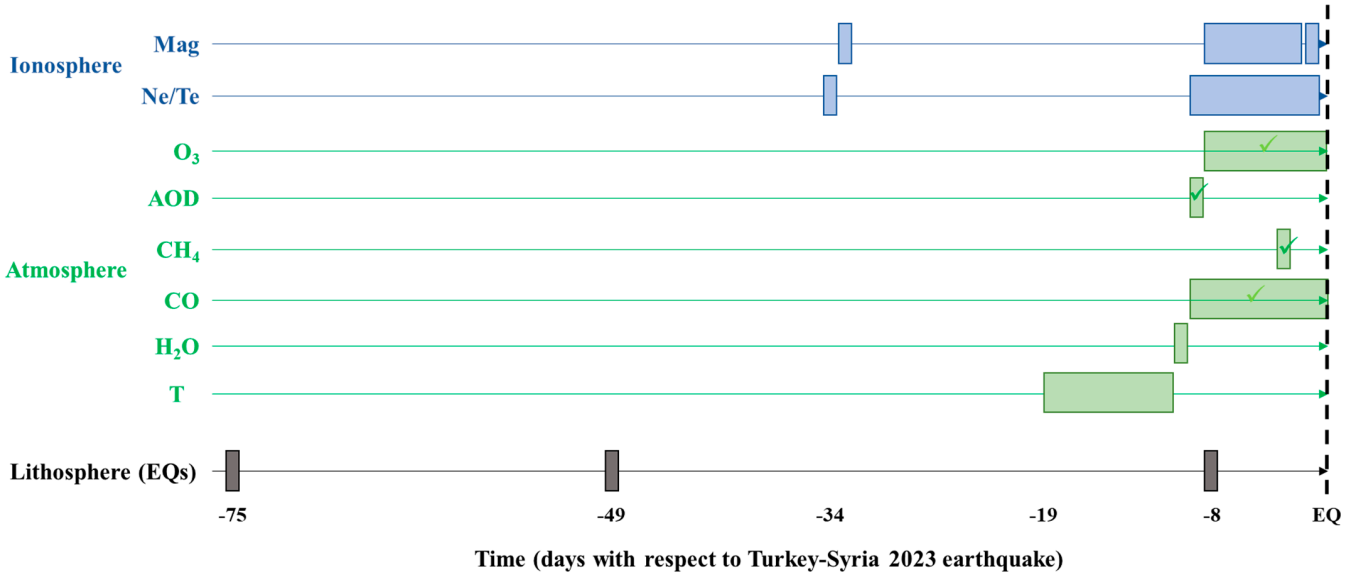

Figure 15. Global view of the identified anomalies in lithosphere atmosphere and ionosphere prior to the Turkey–Syria 2023 earthquake. Each box represents the duration of the identified anomaly (for details, see Table 2). The short names of the atmospheric parameters are T = Surface Temperature, H_2O = Water Vapor and AOD = aerosol optical depth, and the other ones are the analyzed chemical components (carbon monoxide, methane and ozone).

This foreshock would be 117 days before the Turkey–Syria earthquake, and no other anomalies in several layers were found at that time. For atmospheric anomalies, a dark green V-sign (✓) marks the ones that show more spatial correlations with the incoming earthquakes or fault system, as discussed in Section 2.1.2, as well as a light green V-sign that identifies the anomalies that show only partial spatial compatibility.

Given a global look at Figure 15, it is outstanding to note that the seismic precursors are the first ones identified in this chain of anomalies, which agrees with some of the previous results (e.g., [15,20]). Some ionospheric anomalies were identified a little more than one month before the earthquake, similar to the conclusion of Akhoondzadeh and Marchetti [14].

From about 10 days before the Turkey–Syria earthquake, it is possible to see anomalies in all layers and, in particular, 8 days before for lithosphere for the highest number of daily earthquakes that could have released some gases [44] and eventual p-holes [34,49] or radon [48] in the atmosphere, which could have also induced perturbations in the ionosphere, for example, with the formation of plasma bubbles as simulated by Kuo et al. [67].

It is interesting to note that plasma parameters show earlier (2 days) anomalies that could reflect that the altitude of higher ionization (F2) is lower than the magnetic field monitored by Swarm at a higher altitude, so maybe a perturbation that comes from the bottom could alter before the plasma and after the magnetic field at higher altitudes. Globally it is outstanding to note that, in the last days (from about 1.5 weeks until the earthquake), all the layers and parameters showed some anomalies as never seen in the previous month. This supports the idea that the geophysical system was activated in preparation for the incoming catastrophic earthquake.

Despite this, future studies on more earthquakes are necessary to better understand the temporal (and spatial) order of the anomalies that are still not fully clear, and the possible roles of location, focal mechanisms, magnitude, depth, and geology in influencing the ways the lithosphere atmosphere and ionosphere couple together.

5. Conclusions

Currently, the increase and variety of in situ and satellite data possibly related to the preparation phase of earthquakes, different big data processing platforms and the significant growth of anomaly detection algorithms prepared the foundations for creating an earthquake real-time monitoring system, which is a necessary step toward an early warning system (EEW) based on geophysical multiple parametrical observations. In this study, 52 time series, which could contain eventual pre-earthquake anomalies from different data sources, were analyzed over an about period of 6 months.

Clear pre-seismic anomalies were observed from about 10 days before the earthquake until the mainshock. By using the Mamdani FIS-based earthquake system, which was explained in the previous study, the possibility of earthquake prediction from about nine days to one day before the earthquake was tested. Even though the results are promising, we underline that it cannot be considered a prediction because it is a posteriori analysis, made using the epicenter, the magnitude and the interested fault segment by these earthquakes that unfortunately hit Turkey and Syria on February 2023.

It required some non-trivial improvement to transform the system prospectively, and hopefully, one day, it could be used to predict earthquakes mitigating their catastrophic impact, such the one of the events discussed in this paper. In order to better understand the present limitations of this system and to study a way to overpass them, a real-time monitoring geophysical platform, such as the one proposed by Marchetti et al. [65], could be the next step. FIS could be part of such a platform.

In addition, in this paper, it was outstanding to identify a progressive increase in anomaly number starting from about 10 days before and with a particular enhancement the day prior to the mainshock. Such a trend is compatible with a critical system approaching a turning point [68]. In this case, the earthquake behaviour was as found for other significant earthquakes in the World, such as the Amatrice-Norcia (Italy) 2016–2017 seismic activity [20], Ridgecrest (California, USA) 2019 [51] sequences or Kermandec (New Zealand) 2019 earthquake [23]. In fact, in all of these cases, an increase of anomalies toward the earthquake was claimed, as also found clearly in this paper.

Finally, a better understanding of such complex systems can be achieved by a large number of possible pre-earthquake anomalies (i.e., parameters from different layers) used from multiple data sources to reduce uncertainty. In parallel to this empirical work, mathematical and statistical analyses (e.g., [3–5]) are necessary to provide robust shreds of evidence and proof of possible mechanisms for the occurrence of earthquake precursors and their relationship in different layers of the Earth as supported by different theoretical models (e.g., [48,69–71]). It should be noted that solar activity was relatively intense in the studied time period, with a peak about two weeks before the mainshock. The possible trigger of solar and geomagnetic activities of powerful earthquakes has been discussed in different papers, but the results are, in some cases, controversial.

The results of this article, as a preliminary assessment of the behavior of different possible pre-earthquake phenomena before the Turkey 2023 earthquake, could provide

useful suggestions to further researchers studying this and other great earthquakes in the World.

Author Contributions: Conceptualization, methodology, software, data curation, and writing — original draft preparation, M.A.; writing—reviewing and editing, M.A. and D.M.; visualization, M.A. and D.M.; project administration and funding acquisition and validation D.M. All authors have read and agreed to the published version of the manuscript.

Funding: This research was funded by the Chinese Postdoctoral Science Foundation, grant number 2021M691190, for the project "Multiparameter pre-earthquake anomaly study of lithosphere-atmosphere-ionosphere"; and National Natural Science Foundation of China, grant number 41974084 for project "Research on anomaly extraction technology of seismic electromagnetic satellite data based on blind source separation".

Data Availability Statement: Swarm satellite data are freely available by ESA https/ftp server at https://swarm-diss.eo.esa.int/ (accessed on 21 February 2023). The Global USGS earthquake catalogue is freely available from https://earthquake.usgs.gov/earthquakes (accessed on 21 February 2023). Faults represented in Figure 1 were retrieved from European Fault-Source Model 2020 (EFSM20) [24].

Acknowledgments: The authors would like to acknowledge the European Space Agency (ESA) for the Swarm data and the NASA Jet Propulsion Laboratory for the solar and geomagnetic indices. Some analyses and visualizations used in this paper were produced with the Giovanni online data system, developed and maintained by the NASA GES DISC. We also acknowledge the MODIS and AIRS mission scientists and associated NASA personnel for the production of the data used in this research effort. D.M. acknowledges the International Space Science Institute (ISSI at Bern, Switzerland) for supporting International Team 553 led by Essam Ghamry and Zeren Zhima.

Conflicts of Interest: The authors declare no conflict of interest. The funders had no role in the design of the study; in the collection, analyses, or interpretation of data; in the writing of the manuscript, or in the decision to publish the results.

Appendix A. Confutation Analysis in a Comparison Area

In this appendix we present the main analyses made in the Dobrovolsky area of Turkey–Syria 2023 earthquake repeated in a comparison region of the same extension and shifted in longitude, so with center in latitude = 37.166° N (the same of epicenter) and longitude = 30.000° E. This area is in a similar geographical context with the Caspian Sea instead of the Mediterranean but also shows some regional similar characteristics and, overall, is placed in the same hemisphere. The atmospheric analyses in this section were performed with the Giovanni online tool [72] and are reported in Figure A1. The Swarm ionospheric analyses of Ne are reported in Figure A2.

Both atmospheric and ionospheric trends in comparison area do not show any abnormal peak confirming that the anomalies identified in last 1.5 days before the Turkey–Syria 2023 earthquake could be related to its geophysical preparation process.

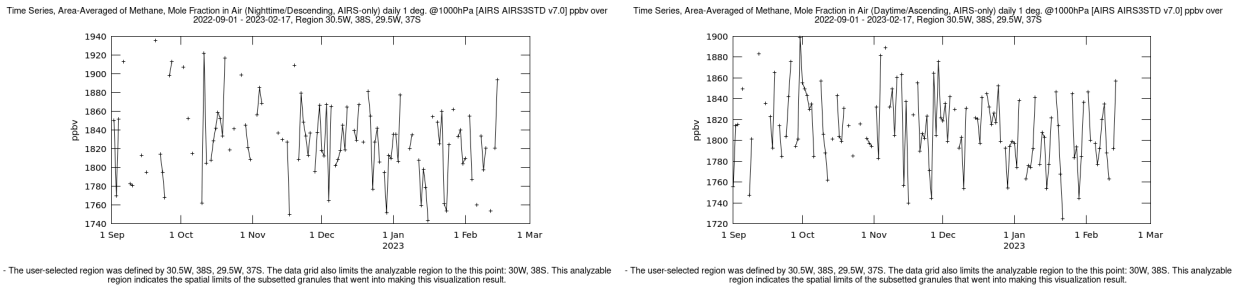

Figure A1. *Cont.*

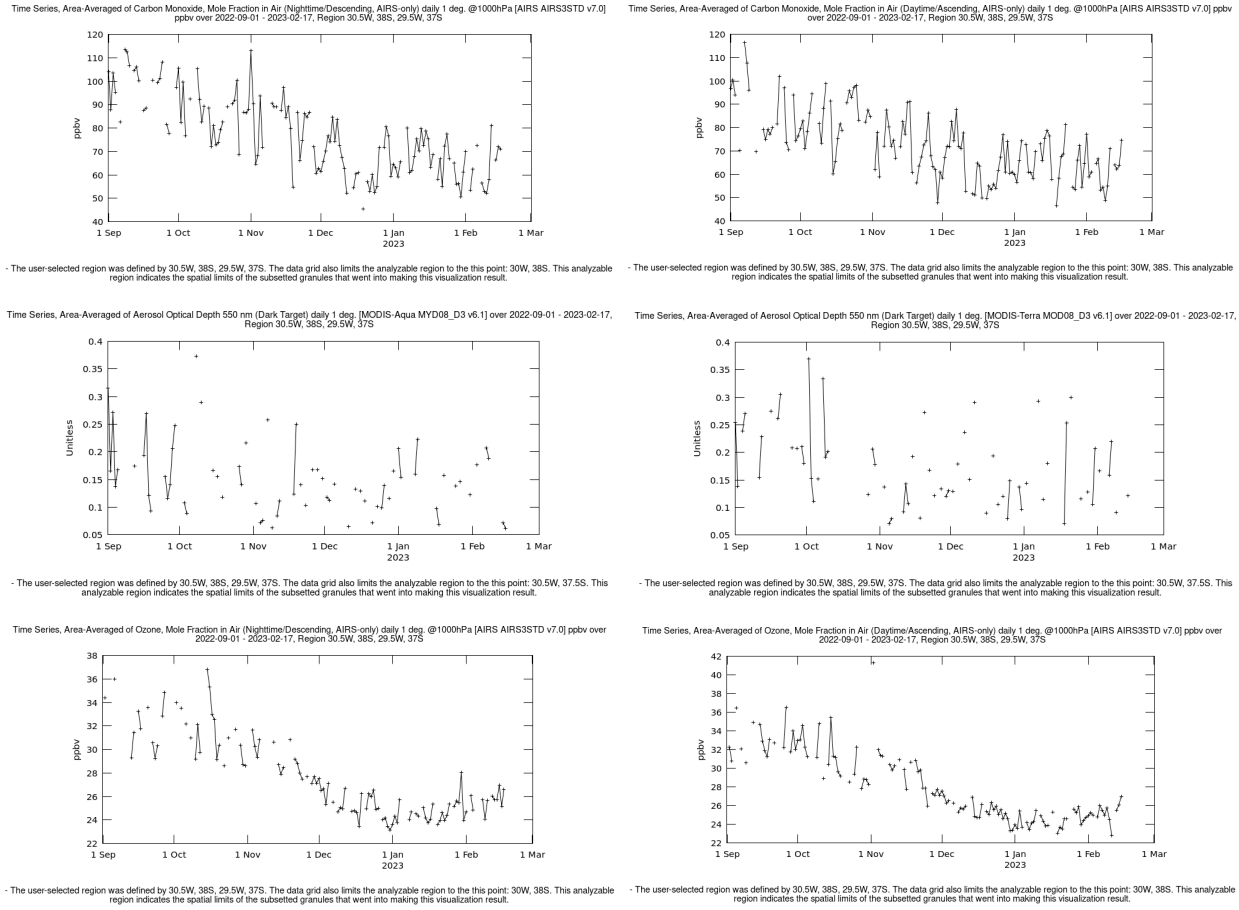

Figure A1. Atmospheric values of methane, carbon monoxide, aerosol and ozone extracted with Giovanni software in comparison area outside the Dobrovolsky circle in the same period of the one analyzed in the manuscript.

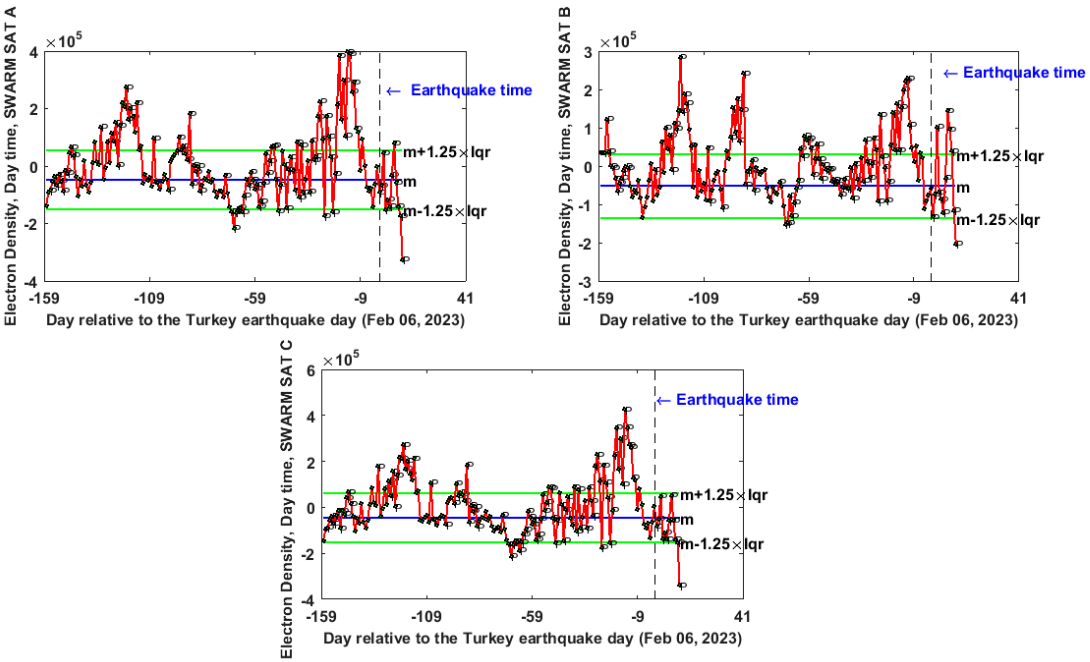

Figure A2. Swarm electron density variations from 1 September 2022 to 17 February 2023 in the comparison area outside the Dobrovolsky area.

Appendix B. Source Identification of Aerosol High Value 9 Days before the Earthquake

In this appendix, we search for the source of the very high peak of aerosol depicted from the time series of Figure 5c 9 days before the Turkey–Syria earthquake (i.e., 28 January 2023). For this purpose, we extracted previous pictures starting from the day before to identify possible other concentrations of aerosol in the surrounding areas as we show in Figure A3. It is possible to note the above Mediterranean Sea there was a very strong cloud of aerosol that moves in north–east direction, overpassing the earthquake region on 28 April 2023.

Considering these conditions, the source of such a strong anomaly seems to not be related to the incoming earthquake. In addition to the previous picture in Figure A4, it is possible to see a wider view of the area only one hour before the first map of Figure A3, i.e., at 10 UT on 27 January 2023. From this picture, the source seems located in Sahara Desert between Egypt and Libya, and the most probable nature of such cloud of aerosol is a sandstorm from the desert, transported by winds above the earthquake area in about one day.

Eventual other sources could be fires, volcanic emissions or other natural or artificial events, but it is excluded that this peak of Figure 5c in the manuscript was caused by the incoming earthquake. Despite this, some smaller aerosol emissions could still be related to the preparation of this earthquake, eventually including the orange pixels in the maps on 28 January at 11UT (see Figure A3) aligned with the plate boundary.

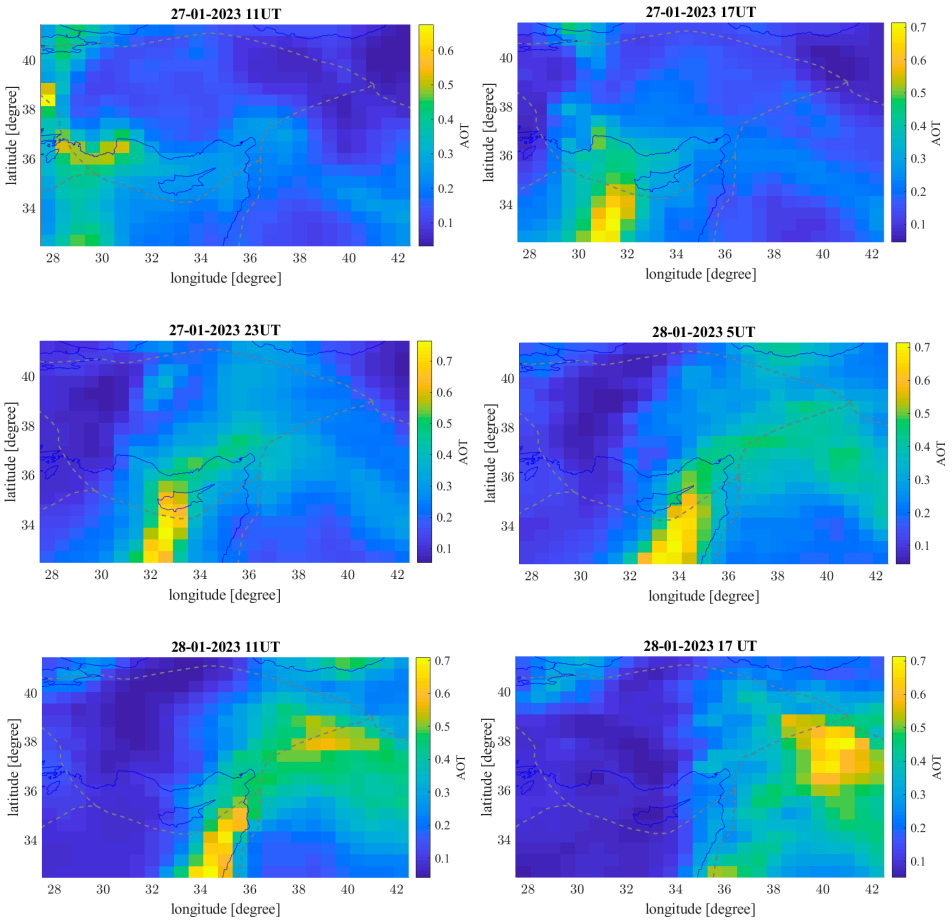

Figure A3. Aerosol maps of 27 January at 11, 17 and 23UT and on to 28 January 2023 at 5, 11 and 17 UT.

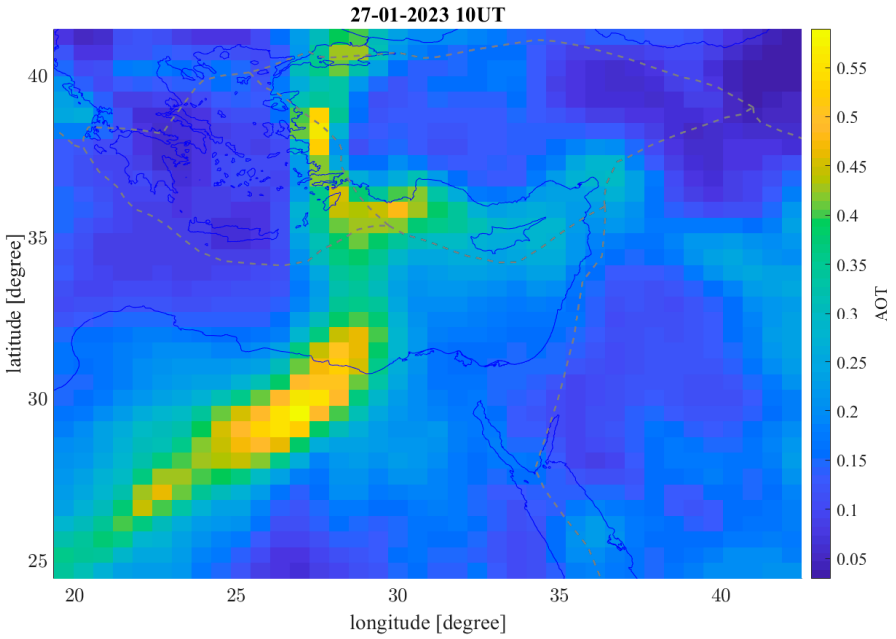

Figure A4. Aerosol maps of 27 January at 10 UT in wider area showing the source of the anomaly detected in Figure 5c.

References

1. Garmaise, M.J.; Moskowitz, T.J. Catastrophic Risk and Credit Markets. *J. Financ.* **2009**, *64*, 657–707. [CrossRef]
2. Mignan, A.; Ouillon, G.; Sornette, D.; Freund, F. Global Earthquake Forecasting System (GEFS): The Challenges Ahead. *Eur. Phys. J. Spec. Top.* **2021**, *230*, 473–490. [CrossRef]
3. De Santis, A.; Marchetti, D.; Pavón-Carrasco, F.J.; Cianchini, G.; Perrone, L.; Abbattista, C.; Alfonsi, L.; Amoruso, L.; Campuzano, S.A.; Carbone, M.; et al. Precursory Worldwide Signatures of Earthquake Occurrences on Swarm Satellite Data. *Sci. Rep.* **2019**, *9*, 20287. [CrossRef]
4. Marchetti, D.; De Santis, A.; Campuzano, S.A.; Zhu, K.; Soldani, M.; D'Arcangelo, S.; Orlando, M.; Wang, T.; Cianchini, G.; Di Mauro, D.; et al. Worldwide Statistical Correlation of Eight Years of Swarm Satellite Data with M5.5+ Earthquakes: New Hints about the Preseismic Phenomena from Space. *Remote Sens.* **2022**, *14*, 2649. [CrossRef]
5. Marchetti, D.; Zhu, K.; Yan, R.; ZeRen, Z.; Shen, X.; Chen, W.; Cheng, Y.; Fan, M.; Wang, T.; Wen, J.; et al. Ionospheric Effects of Natural Hazards in Geophysics: From Single Examples to Statistical Studies Applied to M5.5+ Earthquakes. In Proceedings of the 4th International Electronic Conference on Geosciences, Online, 1–15 December 2022; MDPI: Basel, Switzerland, 2022.
6. Chen, Y.-I.; Huang, C.-S.; Liu, J.-Y. Statistical Evidences of Seismo-Ionospheric Precursors Applying Receiver Operating Characteristic (ROC) Curve on the GPS Total Electron Content in China. *J. Asian Earth Sci.* **2015**, *114*, 393–402. [CrossRef]
7. Genzano, N.; Filizzola, C.; Hattori, K.; Pergola, N.; Tramutoli, V. Statistical Correlation Analysis between Thermal Infrared Anomalies Observed From MTSATs and Large Earthquakes Occurred in Japan (2005–2015). *J. Geophys. Res. Solid Earth* **2021**, *126*, e2020JB020108. [CrossRef]
8. Yan, R.; Parrot, M.; Pinçon, J.-L. Statistical Study on Variations of the Ionospheric Ion Density Observed by DEMETER and Related to Seismic Activities: Ionospheric Density and Seismic Activity. *J. Geophys. Res. Space Phys.* **2017**, *122*, 12,421–12,429. [CrossRef]
9. Akhoondzadeh, M. Advances in Seismo-LAI Anomalies Detection within Google Earth Engine (GEE) Cloud Platform. *Adv. Space Res.* **2022**, *69*, 4351–4357. [CrossRef]
10. Christodoulou, V.; Bi, Y.; Wilkie, G. A Tool for Swarm Satellite Data Analysis and Anomaly Detection. *PLoS ONE* **2019**, *14*, e0212098. [CrossRef] [PubMed]
11. Chen, H.; Han, P.; Hattori, K. Recent Advances and Challenges in the Seismo-Electromagnetic Study: A Brief Review. *Remote Sens.* **2022**, *14*, 5893. [CrossRef]
12. De Santis, A.; Marchetti, D.; Spogli, L.; Cianchini, G.; Pavón-Carrasco, F.J.; Franceschi, G.D.; Di Giovambattista, R.; Perrone, L.; Qamili, E.; Cesaroni, C.; et al. Magnetic Field and Electron Density Data Analysis from Swarm Satellites Searching for Ionospheric Effects by Great Earthquakes: 12 Case Studies from 2014 to 2016. *Atmosphere* **2019**, *10*, 371. [CrossRef]
13. Xiong, P.; Marchetti, D.; De Santis, A.; Zhang, X.; Shen, X. SafeNet: SwArm for Earthquake Perturbations Identification Using Deep Learning Networks. *Remote Sens.* **2021**, *13*, 5033. [CrossRef]
14. Akhoondzadeh, M.; Marchetti, D. Developing a Fuzzy Inference System Based on Multi-Sensor Data to Predict Powerful Earthquake Parameters. *Remote Sens.* **2022**, *14*, 3203. [CrossRef]

15. Zhang, Y.; Wang, T.; Chen, W.; Zhu, K.; Marchetti, D.; Cheng, Y.; Fan, M.; Wang, S.; Wen, J.; Zhang, D.; et al. Are There One or More Geophysical Coupling Mechanisms before Earthquakes? The Case Study of Lushan (China) 2013. *Remote Sens.* **2023**, *15*, 1521. [CrossRef]
16. Ouzounov, D.; Pulinets, S.; Davidenko, D.; Rozhnoi, A.; Solovieva, M.; Fedun, V.; Dwivedi, B.N.; Rybin, A.; Kafatos, M.; Taylor, P. Transient Effects in Atmosphere and Ionosphere Preceding the 2015 M7.8 and M7.3 Gorkha–Nepal Earthquakes. *Front. Earth Sci.* **2021**, *9*, 757358. [CrossRef]
17. Wu, L.; Qi, Y.; Mao, W.; Lu, J.; Ding, Y.; Peng, B.; Xie, B. Scrutinizing and Rooting the Multiple Anomalies of Nepal Earthquake Sequence in 2015 with the Deviation–Time–Space Criterion and Homologous Lithosphere–Coversphere–Atmosphere–Ionosphere Coupling Physics. *Nat. Hazards Earth Syst. Sci.* **2023**, *23*, 231–249. [CrossRef]
18. Ghamry, E.; Mohamed, E.K.; Sekertekin, A.; Fathy, A. Integration of Multiple Earthquakes Precursors before Large Earthquakes: A Case Study of 25 April 2015 in Nepal. *J. Atmos. Sol.-Terr. Phys.* **2023**, *242*, 105982. [CrossRef]
19. Akhoondzadeh, M.; De Santis, A.; Marchetti, D.; Piscini, A.; Cianchini, G. Multi Precursors Analysis Associated with the Powerful Ecuador (MW = 7.8) Earthquake of 16 April 2016 Using Swarm Satellites Data in Conjunction with Other Multi-Platform Satellite and Ground Data. *Adv. Space Res.* **2018**, *61*, 248–263. [CrossRef]
20. Marchetti, D.; De Santis, A.; D'Arcangelo, S.; Poggio, F.; Piscini, A.; Campuzano, S.A.; De Carvalho, W.V.J.O. Pre-Earthquake Chain Processes Detected from Ground to Satellite Altitude in Preparation of the 2016–2017 Seismic Sequence in Central Italy. *Remote Sens. Environ.* **2019**, *229*, 93–99. [CrossRef]
21. Marchetti, D.; De Santis, A.; Shen, X.; Campuzano, S.A.; Perrone, L.; Piscini, A.; Di Giovambattista, R.; Jin, S.; Ippolito, A.; Cianchini, G.; et al. Possible Lithosphere-Atmosphere-Ionosphere Coupling Effects Prior to the 2018 Mw = 7.5 Indonesia Earthquake from Seismic, Atmospheric and Ionospheric Data. *J. Asian Earth Sci.* **2020**, *188*, 104097. [CrossRef]
22. Akhoondzadeh, M.; De Santis, A.; Marchetti, D.; Shen, X. Swarm-TEC Satellite Measurements as a Potential Earthquake Precursor Together with Other Swarm and CSES Data: The Case of Mw7.6 2019 Papua New Guinea Seismic Event. *Front. Earth Sci.* **2022**, *10*, 820189. [CrossRef]
23. De Santis, A.; Perrone, L.; Calcara, M.; Campuzano, S.A.; Cianchini, G.; D'Arcangelo, S.; Di Mauro, D.; Marchetti, D.; Nardi, A.; Orlando, M.; et al. A Comprehensive Multiparametric and Multilayer Approach to Study the Preparation Phase of Large Earthquakes from Ground to Space: The Case Study of the June 15 2019, M7.2 Kermadec Islands (New Zealand) Earthquake. *Remote Sens. Environ.* **2022**, *283*, 113325. [CrossRef]
24. Basili, R.; Danciu, L.; Beauval, C.; Sesetyan, K.; Vilanova, S.; Adamia, S.; Arroucau, P.; Atanackov, J.; Baize, S.; Canora, C.; et al. *European Fault-Source Model 2020 (EFSM20): Online Data on Fault Geometry and Activity Parameters*; Istituto Nazionale Di Geofisica e Vulcanologia (INGV): Rome, Italy, 2022. [CrossRef]
25. Pulinets, S.; Ouzounov, D.; Karelin, A.; Boyarchuk, K. *Earthquake Precursors in the Atmosphere and Ionosphere: New Concepts*; Springer: Dordrecht, The Netherlands, 2022; ISBN 978-94-024-2170-5.
26. Liu, J.Y.; Chuo, Y.J.; Shan, S.J.; Tsai, Y.B.; Chen, Y.I.; Pulinets, S.A.; Yu, S.B. Pre-Earthquake Ionospheric Anomalies Registered by Continuous GPS TEC Measurements. *Ann. Geophys.* **2004**, *22*, 1585–1593. [CrossRef]
27. Tertyshinikov, A.V. The Variations of Ozone Content in the Atmosphere above Strong Earthquake Epicenter. *Izv. Phys. Solid Earth* **1995**, *31*, 789–794.
28. Tronin, A.A. Remote Sensing and Earthquakes: A Review. *Phys. Chem. Earth Parts A/B/C* **2006**, *31*, 138–142. [CrossRef]
29. Piscini, A.; De Santis, A.; Marchetti, D.; Cianchini, G. A Multi-Parametric Climatological Approach to Study the 2016 Amatrice–Norcia (Central Italy) Earthquake Preparatory Phase. *Pure Appl. Geophys.* **2017**, *174*, 3673–3688. [CrossRef]
30. Cui, Y.; Zheng, C.; Jiang, L.; Huang, J.; Sun, F.; Zou, Z.; Du, J. Variations of Multiple Gaseous Emissions Associated with the Great Sumatra Earthquakes in 2004 and 2005. *Chem. Geol.* **2023**, *618*, 121311. [CrossRef]
31. Scholz, C.H.; Sykes, L.R.; Aggarwal, Y.P. Earthquake Prediction: A Physical Basis. *Science* **1973**, *181*, 803–810. [CrossRef]
32. Chiodini, G.; Cardellini, C.; Amato, A.; Boschi, E.; Caliro, S.; Frondini, F.; Ventura, G. Carbon Dioxide Earth Degassing and Seismogenesis in Central and Southern Italy: Carbon Dioxide Earth Degassing and Seismogenesis. *Geophys. Res. Lett.* **2004**, *31*, 1–4. [CrossRef]
33. Di Luccio, F.; Ventura, G.; Di Giovambattista, R.; Piscini, A.; Cinti, F.R. Normal Faults and Thrusts Reactivated by Deep Fluids: The 6 April 2009 M_w 6.3 L'Aquila Earthquake, Central Italy. *J. Geophys. Res.* **2010**, *115*, B06315. [CrossRef]
34. Freund, F. Pre-Earthquake Signals: Underlying Physical Processes. *J. Asian Earth Sci.* **2011**, *41*, 383–400. [CrossRef]
35. Etiope, G.; Martinelli, G. Migration of Carrier and Trace Gases in the Geosphere: An Overview. *Phys. Earth Planet. Inter.* **2002**, *129*, 185–204. [CrossRef]
36. Ganguly, N.D. Variation in Atmospheric Ozone Concentration Following Strong Earthquakes. *Int. J. Remote Sens.* **2009**, *30*, 349–356. [CrossRef]
37. Filizzola, C.; Corrado, A.; Genzano, N.; Lisi, M.; Pergola, N.; Colonna, R.; Tramutoli, V. RST Analysis of Anomalous TIR Sequences in Relation with Earthquakes Occurred in Turkey in the Period 2004–2015. *Remote Sens.* **2022**, *14*, 381. [CrossRef]
38. Tramutoli, V.; Cuomo, V.; Filizzola, C.; Pergola, N.; Pietrapertosa, C. Assessing the Potential of Thermal Infrared Satellite Surveys for Monitoring Seismically Active Areas: The Case of Kocaeli (İzmit) Earthquake, August 17, 1999. *Remote Sens. Environ.* **2005**, *96*, 409–426. [CrossRef]
39. Jing, F.; Zhang, L.; Singh, R.P. Pronounced Changes in Thermal Signals Associated with the Madoi (China) M 7.3 Earthquake from Passive Microwave and Infrared Satellite Data. *Remote Sensing* **2022**, *14*, 2539. [CrossRef]

40. Tronin, A.A. Satellite Thermal Survey—A New Tool for the Study of Seismoactive Regions. *Int. J. Remote Sens.* **1996**, *17*, 1439–1455. [CrossRef]
41. Saradjian, M.R.; Akhoondzadeh, M. Thermal Anomalies Detection before Strong Earthquakes ($M > 6.0$) Using Interquartile, Wavelet and Kalman Filter Methods. *Nat. Hazards Earth Syst. Sci.* **2011**, *11*, 1099–1108. [CrossRef]
42. Qiang, Z.; Xu, X.; Dian, C. Case 27 Thermal Infrared Anomaly Precursor of Impending Earthquakes. *Pure Appl. Geophys.* **1997**, *149*, 159–171. [CrossRef]
43. Chiodini, G.; Cardellini, C.; Di Luccio, F.; Selva, J.; Frondini, F.; Caliro, S.; Rosiello, A.; Beddini, G.; Ventura, G. Correlation between Tectonic CO_2 Earth Degassing and Seismicity Is Revealed by a 10-Year Record in the Apennines, Italy. *Sci. Adv.* **2020**, *6*, eabc2938. [CrossRef] [PubMed]
44. Enomoto, Y. Coupled Interaction of Earthquake Nucleation with Deep Earth Gases: A Possible Mechanism for Seismo-Electromagnetic Phenomena. *Geophys. J. Int.* **2012**, *191*, 1210–1214. [CrossRef]
45. Singh, R.P.; Senthil Kumar, J.; Zlotnicki, J.; Kafatos, M. Satellite Detection of Carbon Monoxide Emission Prior to the Gujarat Earthquake of 26 January 2001. *Appl. Geochem.* **2010**, *25*, 580–585. [CrossRef]
46. Tamburello, G.; Pondrelli, S.; Chiodini, G.; Rouwet, D. Global-Scale Control of Extensional Tectonics on CO2 Earth Degassing. *Nat. Commun.* **2018**, *9*, 4608. [CrossRef]
47. Romaniello, V.; Piscini, A.; Bignami, C.; Anniballe, R.; Stramondo, S. Earthquake Damage Mapping by Using Remotely Sensed Data: The Haiti Case Study. *J. Appl. Remote Sens.* **2017**, *11*, 016042. [CrossRef]
48. Pulinets, S.; Ouzounov, D. Lithosphere–Atmosphere–Ionosphere Coupling (LAIC) Model—An Unified Concept for Earthquake Precursors Validation. *J. Asian Earth Sci.* **2011**, *41*, 371–382. [CrossRef]
49. Freund, F.; Ouillon, G.; Scoville, J.; Sornette, D. Earthquake Precursors in the Light of Peroxy Defects Theory: Critical Review of Systematic Observations. *Eur. Phys. J. Spec. Top.* **2021**, *230*, 7–46. [CrossRef]
50. Pulinets, S.A.; Alekseev, V.A.; Legen'ka, A.D.; Khegai, V.V. Radon and Metallic Aerosols Emanation before Strong Earthquakes and Their Role in Atmosphere and Ionosphere Modification. *Adv. Space Res.* **1997**, *20*, 2173–2176. [CrossRef]
51. De Santis, A.; Cianchini, G.; Marchetti, D.; Piscini, A.; Sabbagh, D.; Perrone, L.; Campuzano, S.A.; Inan, S. A Multiparametric Approach to Study the Preparation Phase of the 2019 M7.1 Ridgecrest (California, United States) Earthquake. *Front. Earth Sci.* **2020**, *8*, 540398. [CrossRef]
52. Marchetti, D.; Zhu, K.; Zhang, H.; Zhima, Z.; Yan, R.; Shen, X.; Chen, W.; Cheng, Y.; He, X.; Wang, T.; et al. Clues of Lithosphere, Atmosphere and Ionosphere Variations Possibly Related to the Preparation of La Palma 19 September 2021 Volcano Eruption. *Remote Sens.* **2022**, *14*, 5001. [CrossRef]
53. Zhang, X.; Murakami, T.; Wang, J.; Aikawa, M. Sources, Species and Secondary Formation of Atmospheric Aerosols and Gaseous Precursors in the Suburb of Kitakyushu, Japan. *Sci. Total Environ.* **2021**, *763*, 143001. [CrossRef]
54. Ventura, G.; Di Giovambattista, R. Fluid Pressure, Stress Field and Propagation Style of Coalescing Thrusts from the Analysis of the 20 May 2012 M_L 5.9 Emilia Earthquake (Northern Apennines, Italy): Propagation Style of Coalescing Thrusts. *Terra Nova* **2013**, *25*, 72–78. [CrossRef]
55. Marchetti, D.; Akhoondzadeh, M. Analysis of Swarm Satellites Data Showing Seismo-Ionospheric Anomalies around the Time of the Strong Mexico (Mw = 8.2) Earthquake of 08 September 2017. *Adv. Space Res.* **2018**, *62*, 614–623. [CrossRef]
56. Akhoondzadeh, M.; De Santis, A.; Marchetti, D.; Piscini, A.; Jin, S. Anomalous Seismo-LAI Variations Potentially Associated with the 2017 Mw = 7.3 Sarpol-e Zahab (Iran) Earthquake from Swarm Satellites, GPS-TEC and Climatological Data. *Adv. Space Res.* **2019**, *64*, 143–158. [CrossRef]
57. Akhoondzadeh, M.; De Santis, A.; Marchetti, D.; Wang, T. Developing a Deep Learning-Based Detector of Magnetic, Ne, Te and TEC Anomalies from Swarm Satellites: The Case of Mw 7.1 2021 Japan Earthquake. *Remote Sens.* **2022**, *14*, 1582. [CrossRef]
58. Marchitelli, V.; Harabaglia, P.; Troise, C.; De Natale, G. On the Correlation between Solar Activity and Large Earthquakes Worldwide. *Sci. Rep.* **2020**, *10*, 11495. [CrossRef]
59. Akhoondzadeh, M.; De Santis, A. Is the Apparent Correlation between Solar-Geomagnetic Activity and Occurrence of Powerful Earthquakes a Casual Artifact? *Atmosphere* **2022**, *13*, 1131. [CrossRef]
60. Dobrovolsky, I.P.; Zubkov, S.I.; Miachkin, V.I. Estimation of the Size of Earthquake Preparation Zones. *Pure Appl. Geophys.* **1979**, *117*, 1025–1044. [CrossRef]
61. Zhu, K.; Fan, M.; He, X.; Marchetti, D.; Li, K.; Yu, Z.; Chi, C.; Sun, H.; Cheng, Y. Analysis of Swarm Satellite Magnetic Field Data Before the 2016 Ecuador (Mw = 7.8) Earthquake Based on Non-Negative Matrix Factorization. *Front. Earth Sci.* **2021**, *9*, 621976. [CrossRef]
62. Alken, P.; Thébault, E.; Beggan, C.D.; Amit, H.; Aubert, J.; Baerenzung, J.; Bondar, T.N.; Brown, W.J.; Califf, S.; Chambodut, A.; et al. International Geomagnetic Reference Field: The Thirteenth Generation. *Earth Planets Space* **2021**, *73*, 49. [CrossRef]
63. Rostami, A.; Akhoondzadeh, M.; Amani, M. A Fuzzy-Based Flood Warning System Using 19-Year Remote Sensing Time Series Data in the Google Earth Engine Cloud Platform. *Adv. Space Res.* **2022**, *70*, 1406–1428. [CrossRef]
64. Mamdani, E.H. Application of Fuzzy Algorithms for Control of Simple Dynamic Plant. *Proc. Inst. Electr. Eng.* **1974**, *121*, 1585. [CrossRef]
65. Marchetti, D.; Zhu, K.; Marchetti, L.; Zhang, Y.; Chen, W.; Cheng, Y.; Fan, M.; Wang, S.; Wang, T.; Wen, J.; et al. Quick Report on the ML = 3.3 on 1 January 2023 Guidonia (Rome, Italy) Earthquake: Evidence of a Seismic Acceleration. *Remote Sens.* **2023**, *15*, 942. [CrossRef]

66. Campuzano, S.A.; De Santis, A.; Pavón-Carrasco, F.J.; Osete, M.L.; Qamili, E. New Perspectives in the Study of the Earth's Magnetic Field and Climate Connection: The Use of Transfer Entropy. *PLoS ONE* **2018**, *13*, e0207270. [CrossRef]
67. Kuo, C.L.; Lee, L.C.; Huba, J.D. An Improved Coupling Model for the Lithosphere-Atmosphere-Ionosphere System. *J. Geophys. Res. Space Phys.* **2014**, *119*, 3189–3205. [CrossRef]
68. De Santis, A.; Abbattista, C.; Alfonsi, L.; Amoruso, L.; Campuzano, S.A.; Carbone, M.; Cesaroni, C.; Cianchini, G.; De Franceschi, G.; De Santis, A.; et al. Geosystemics View of Earthquakes. *Entropy* **2019**, *21*, 412. [CrossRef]
69. Molchanov, O.A.; Hayakawa, M. Generation of ULF Electromagnetic Emissions by Microfracturing. *Geophys. Res. Lett.* **1995**, *22*, 3091–3094. [CrossRef]
70. Hayakawa, M.; Kasahara, Y.; Nakamura, T.; Hobara, Y.; Rozhnoi, A.; Solovieva, M.; Molchanov, O.; Korepanov, V. Atmospheric Gravity Waves as a Possible Candidate for Seismo-Ionospheric Perturbations. *J. Atmospheric Electr.* **2011**, *31*, 129–140. [CrossRef]
71. Liperovsky, V.A.; Pokhotelov, O.A.; Meister, C.-V.; Liperovskaya, E.V. Physical Models of Coupling in the Lithosphere-Atmosphere-Ionosphere System before Earthquakes. *Geomagn. Aeron.* **2008**, *48*, 795–806. [CrossRef]
72. Acker, J.G.; Leptoukh, G. Online Analysis Enhances Use of NASA Earth Science Data. *Eos Trans. AGU* **2007**, *88*, 14. [CrossRef]